SCHOOL OF ADVANCED STUDIES OF THE ROMANIAN ACADEMY

DOCTORAL SCHOOL OF CHEMICAL SCIENCES

„PETRU PONI" INSTITUTE OF MACROMOLECULAR CHEMISTRY

Field of study: CHEMISTRY

IN SILICO STUDIES OF DYNAMICAL SELF-ASSEMBLY IN CONTROLLED DRUG DELIVERY AND RELEASE

SUMMARY OF DOCTORAL THESIS

SCIENTIFIC COORDINATOR:

PROF. DR. AATTO LAAKSONEN

Ph.D. STUDENT:

PETRU TÎRNOVAN

2026

Acknowledgements

This doctoral thesis represents the culmination of years of continuous learning and professional development, as well as the synthesis of the knowledge I have acquired and applied in the field of theoretical chemistry. The completion of my doctoral studies marks the end of an important stage in my early career as a researcher, while also serving as a starting point for exploring a much broader scientific horizon.

I would like to express my sincere gratitude to my doctoral supervisor, **Prof. Dr. Aatto Laaksonen**, for his guidance and for providing access to valuable scientific resources throughout this stage of my academic journey.

I adress my deepest appreciation to **CS I Dr. Mariana Pinteală**, for her guidance, moral and logistical support, and unwavering patience throughout my doctoral studies, with an essential role into reaching this milestone.

I am profoundly grateful to **Dr. Narcisa-Laura Marangoci** and **Dr. Dragoș-Lucian** Isac for their guidance in my research activities, the opportunities for scientific collaboration, and their continuous support throughout the preparation of this doctoral thesis.

I would like to express my gratitude to **Prof. Dr. Francesca Mocci** from the **University of Cagliari**, Italy, for her assistance in the application of computational methods, and to **Prof. Dr. Elena Simona Băcăiță** from the **Gheorghe Asachi Technical University** of Iași, for her support and the valuable scientific collaboration established during this period.

I thank all my colleagues from **IntelCentru** for their ideas, advice, and support.

I wish to acknowledge the **Romanian Academy** and the **Petru Poni Institute of Macromolecular Chemistry** for providing me with the opportunity to pursue my doctoral studies and for granting access to the research infrastructure necessary to carry out my scientific work.

The research presented in this doctoral thesis was financially supported by the following research projects: **„Intelligent systems for cancer diagnosis and treatment - IntelDots" PNRR-III-C9-2022-I8-291** and "**BioMat4CAST - Petru Poni Institute of Macromolecular Chemistry Multi-Scale In Silico Laboratory for Complex and Smart Biomaterials", Grant Agreement No. 101086667.**

Also, I would like to thank **FreeYaMind Campus** for providing access to quantum computing courses and the associated computational infrastructure.

Last but not least, I am deeply grateful to **my family** for their unwavering emotional support, continuous sacrifices, and essential contribution to everything I have achieved throughout these years.

With gratitude,

Ph.D. student Petru Tîrnovan

TABLE OF CONTENTS

LIST OF ABBREVIATIONS

INTRODUCTION 1

PART I: CURRENT STATE OF RESEARCH IN THE FIELD OF THE DOCTORAL THESIS 4

CHAPTER I. THE IMPORTANCE OF SELF-ASSEMBLED SYSTEMS IN THE DELIVERY OF PHARMACEUTICAL FORMULATIONS 4

I.1. General Principles. Literature Review. 4

I.2. Theoretical Chemistry Methods Applied to the Study of Drug Delivery Systems 13

I.2.1. Quantum Chemistry Methods 13

I.2.1.1. Ab initio methods 17

I.2.1.2. Density Functional Theory Method 23

I.2.2. Molecular Docking Method 27

I.2.3. Molecular Dynamics Methods 28

I.2.4. Umbrella Sampling Method. Potential of Mean Force (PMF) 34

I.3. Cyclodextrin-Based Systems with Potential Applications in Drug Delivery 37

I.3.1. Cyclodextrins. Definition. Structure. Characterization. 37

I.3.2. Applications of Cyclodextrins in the Delivery of Pharmaceutical Formulations 39

I.4. PNIPAM-Based Systems with Potential Applications in Drug Delivery 42

I.5. Graphene-Based Systems with Potential Applications in Drug Delivery 45

PART II: ORIGINAL CONTRIBUTIONS 49

CHAPTER II. β-CYCLODEXTRIN-BASED INCLUSION COMPLEXES 49

II.1. PROPICONAZOLE/CYCLODEXTRIN INCLUSION COMPLEXES (PCZH-NO_3/β-CD): THE ROLE OF THE COSOLVENT 49

II.1.1. Introduction: Rationale and Objectives of the Study 49

II.1.2. Materials and Methods 54

II.1.2.1. Materials and Methods used in the Experimental Study 54

II.1.2.2. Molecular Dynamics Studies 54

II.1.3. Results and Discussions 55

II.1.4. Conclusions 74

II. 2. 2,6-DIAMINO-1-N-HYDROXY-4-(PYRROLIDIN-1′-YL)PYRIMIDIN-1-IUM L-2-OXOTHIAZOLINE-4-CARBOXYLATE (MPPC)/β-CD INCLUSION COMPLEXES: THE ROLE OF ORGANIC IONS 75

II.2.1. Introduction: Rationale and Objectives of the Study 75

II.2.2. Materials and Methods 78
II.2.2.1. Materials and Experimental Methods 78
II.2.2.2. Computational Methods 81
II.2.3. Results and Discussions 87
II.2.3.1. Theoretical Results and Discussions 87
II.2.3.2. Experimental Results and Discussions 96
II.2.4. Conclusions 108
CHAPTER III. MOLECULAR SYSTEMS WITH POTENTIAL APPLICATIONS IN DRUG DELIVERY: IN SILICO STUDIES ON THE INFLUENCE OF THE SOLVATION MODEL ON THE LOWER CRITICAL SOLUTION TEMPERATURE (LCST) OF PNIPAM-BASED STIMULI-RESPONSIVE POLYMERS 110
III.1. Introduction: Rationale and Objectives of the Study 110
III.2. Computational Methods 114
III.3. Results and Discussions 118
III.4. Conclusions 138
CHAPTER IV. MOLECULAR SYSTEMS WITH POTENTIAL APPLICATIONS IN BIOIMAGING: A TD-DFT STUDY ON THE INFLUENCE OF MOLECULAR STRUCTURE ON THE ABSORPTION WAVELENGTH OF POLYCYCLIC AROMATIC HYDROCARBONS (PAHs) AND GRAPHENE QUANTUM DOTS (GQDs) 140
IV.1. Introduction: Rationale and Objectives of the Study 140
IV.2. Computational Methods 142
IV.3. Results and Discussions 146
IV.4. Conclusions 174
GENERAL CONCLUSIONS 177
BIBLIOGRAPHY 184
APPENDIX 1. DISSEMINATION OF RESEARCH RESULTS
APPENDIX 2. DATASETS GENERATED FROM THE THEORETICAL STUDIES PRESENTED IN CHAPTER IV

INTRODUCTION

Drug delivery and controlled-release systems represent one of the major areas of modern medicine, playing an essential role in improving therapeutic efficacy and reducing the adverse effects associated with conventional treatments. In traditional medical practice, drug administration often results in systemic distribution, regardless of whether the therapeutic target is located within a specific organ, tissue, or cell type. This nonspecific distribution may lead to substantial losses of the active pharmaceutical ingredient, necessitating the administration of higher doses and potentially causing undesirable side effects, particularly in the case of highly toxic compounds or drugs with a narrow therapeutic window. In this context, the development of systems capable of encapsulating active pharmaceutical ingredients, their transport to the targeted site, and releasing them in a controlled manner has become a priority in the contemporary biomedical research.

Over the past decades, advances in materials science, nanotechnology, polymer chemistry, and biotechnology have enabled the development of sophisticated drug delivery platforms. These include polymeric nanoparticles, liposomes, micelles, hydrogels, dendrimers, nanocapsules, inorganic material-based systems, and drug-polymer conjugates. These systems can be designed to protect active pharmaceutical ingredients from enzymatic or chemical degradation, improve their solubility, prolong their circulation time in the body, and facilitate their accumulation in affected tissues. Furthermore, through surface functionalization with specific ligands, antibodies, peptides, or other recognition molecules, drug carriers can acquire the ability to interact selectively with particular cells or biological structures, thereby enabling the targeted delivery of active pharmaceutical ingredients to the affected site.

Investigating the interactions that govern the properties of these systems is of paramount importance, as the resulting data can provide valuable insights into their potential efficacy and mechanisms of action in biological environments. In recent years, in silico methods have emerged as robust and efficient tools for investigating such systems, leveraging the computational power of high-performance computing resources equipped with large numbers of central processing units (CPUs) and graphics processing units (GPUs). By integrating computational approaches with experimental analysis and validation, researchers can accelerate the design, development, and optimization of chemical systems capable of drug delivery, while reducing the time, financial costs, materials, and chemical reagents typically required for laboratory experiments. Furthermore, this integrated approach contributes to the

principles of the circular economy by promoting more efficient resource utilization and minimizing material consumption and waste generation.

In conclusion, the development of systems capable of delivering and releasing active compounds in a controlled manner requires an understanding of the molecular processes governing their stability, selectivity, and response to environmental conditions. The complexation of an active compound, the conformational reorganization of a polymer, or changes in the electronic structure of a nanomaterial can influence properties relevant to biomedical applications. Investigating these processes at the molecular level provides valuable insights for the design and optimization of drug delivery systems and bioimaging materials.

The doctoral thesis entitled " ***IN SILICO*** **STUDIES OF DYNAMICAL SELF-ASSEMBLY IN CONTROLLED DRUG DELIVERY AND RELEASE**" aims to investigate, using complementary *in silico* methods, the relationships between molecular structure, molecular interactions, and the properties of systems with potential applications in the delivery and controlled release of active pharmaceutical ingredients or in bioimaging. The research focuses on elucidating complexation mechanisms, characterizing conformational responses to temperature, and evaluating the influence of structural modifications on optical properties. To this end, three classes of systems are investigated: β-cyclodextrin-based inclusion complexes, thermoresponsive poly(N-isopropylacrylamide) (PNIPAM) polymers, and graphene quantum dots (GQDs).

The thesis is structured into two parts. **Part I**, dedicated to the current state of research, comprises **Chapter I**, which presents a literature review of the main classes of systems employed for the delivery and controlled release of active pharmaceutical ingredients, with particular emphasis on inclusion complexes, stimuli-responsive polymers, and graphene-based materials. The literature analysis highlights that the properties of drug delivery systems depend on host–guest interactions, conformational responses to environmental conditions, and the structural characteristics of the materials involved. Characterizing these processes requires complementary methods capable of describing both molecular dynamics and electronic structure. Furthermore, this chapter outlines the theoretical chemistry methods employed to investigate these systems and establishes the conceptual framework for the original research presented in Part II, which comprises **Chapters II-IV**.

Chapter II focuses on β-cyclodextrin-based inclusion complexes and aims to identify the factors governing the orientation, selectivity, and stability of host–guest associations. The first study examines the influence of water–dimethyl sulfoxide mixture composition on the

complexation of propiconazole nitrate (PCZH-NO_3), emphasizing the competition between the cosolvent and the guest molecule for occupancy of the cyclodextrin cavity. The second study investigates the complexation of the ionic formulation MPPC, the active ingredient in Minoxicapil®, focusing on the distinct behavior of the cation and anion during their interactions with β-cyclodextrin. The theoretical results are correlated with experimental measurements to characterize the inclusion mechanisms and the intermolecular interactions involved.

Chapter III addresses the thermoresponsive behavior of PNIPAM, a polymer with potential applications in the development of controlled drug delivery systems. Molecular dynamics simulations are employed to investigate the influence of the water model and the number of polymer chains on hydration, interchain interactions, and the transition from extended to compact conformations. The study aims to identify the simulation conditions and molecular descriptors suitable for characterizing this transition near the lower critical solution temperature (LCST), as well as to elucidate the role of hydrogen bonding in the polymer collapse process.

Chapter IV investigates the relationship between molecular structure and the optical absorption properties of polycyclic aromatic hydrocarbons and graphene quantum dots. The effects of size, edge type, number of layers, functionalization, and structural defects on the positions of absorption bands are systematically examined. Considering the structural complexity of experimentally synthesized GQDs, the study employs molecular models to investigate how structural modifications influence optical responses. The results provide insights into the design of materials with tunable optical properties, relevant to the future development of bioimaging applications, while their potential use in drug delivery remains a prospect requiring further investigation.

The selection of in silico methods reflects the need to describe the investigated processes at both the atomistic and electronic levels. In **Chapter II**, molecular docking enables the exploration of binding configurations, molecular dynamics simulations are used to monitor the evolution of the complexes and their interactions with the solvent, and umbrella sampling allows the construction of free energy profiles associated with complexation. In **Chapter III**, molecular dynamics simulations are employed to characterize the hydration and conformational reorganization of PNIPAM systems as a function of temperature. In **Chapter IV**, density functional theory (DFT) and its time-dependent extension (TD-DFT) enable the investigation of electronic structure and electronic transitions from the ground state to excited states. Through their complementary capabilities, these methods provide mechanistic

explanations for processes that are difficult to investigate directly through experiments and allow theoretical predictions to be compared with experimental measurements, where available.

CHAPTER II. β-CYCLODEXTRIN-BASED INCLUSION COMPLEXES

II.1. PROPICONAZOLE/CYCLODEXTRIN INCLUSION COMPLEXES (PCZH-NO3/β-CD): THE ROLE OF THE COSOLVENT

The study of the inclusion complex formed between propiconazole nitrate and β-cyclodextrin was motivated by the need to improve antifungal formulations and enhance their therapeutic efficacy. Propiconazole is an azole compound with significant antifungal activity (Fifere et al., 2012; Marangoci et al., 2011), however, its physicochemical properties may limit its optimal use in certain formulations.. β-cyclodextrin was selected as the host system due to its ability to accommodate molecular fragments of propiconazole within its hydrophobic cavity. The formation of such an inclusion complex may contribute to improving the stability, solubility, and bioavailability of the active pharmaceutical ingredient. (Pricope et al., 2018).

The **scope of the study** was to evaluate the influence of water-dimethyl sulfoxide (DMSO) mixture composition on the formation and stability of the propiconazole nitrate/β-cyclodextrin complex. The investigation focused on the role of DMSO in the complexation process, as it can interact with both the host and guest molecules and compete for occupancy of the cyclodextrin cavity (Isac et al., 2025). To elucidate this mechanism, molecular dynamics simulations and free energy profile calculations were performed, and the theoretical results were correlated with experimental data obtained through nuclear magnetic resonance (NMR) spectroscopy.

The **original contribution** lies in the molecular-level description of the competition between DMSO, water, and propiconazole nitrate for occupancy of the β-cyclodextrin cavity, as well as in the characterization of the influence of solvent composition on the thermodynamic favorability of complexation. The combined theoretical and experimental approach enabled the correlation of the dynamic behavior of molecules within the cavity with changes in the binding affinity of the guest molecule.

The **results** obtained demonstrate that DMSO molecules dynamically occupy the β-cyclodextrin cavity and compete with propiconazole nitrate for inclusion. Increasing the proportion of DMSO within the investigated range leads to less negative complexation free energy values, indicating a less favorable association, whereas mixtures containing lower proportions of DMSO favor complex formation. These findings clarify the role of the cosolvent in the inclusion mechanism and provide guidance for selecting suitable

complexation media in the development of propiconazole nitrate and β-cyclodextrin-based formulations.

II.1.3. Results and discussions

In any complexation process, the dominant intermolecular interactions play a crucial role in determining its direction and progression. The main governing factors are the properties of the target compound and those of the solvent/cosolvent system. Furthermore, the properties of cyclodextrin (CD), including its size and conformational dynamics, influence these interactions, while structural changes may occur in response to variations in the solvent/cosolvent ratio.

To evaluate these changes, the root-mean-square deviation (RMSD) of free β-CD, in the absence of PCZH-NO_3, was calculated in both pure solvents and DMSO/water mixtures. The results are presented in **Figure II.1.2**. The RMSD values calculated for all atoms of β-CD showed no significant variations across the different DMSO/water ratios: 0,11 ± 0,027 nm in pure water, 0,11 ± 0,022 nm in pure DMSO, 0,12 ± 0,026 nm at 5 % v/v, 0,11 ± 0,023 nm at 10 % v/v, 0,097 ± 0,019 nm at 20 % v/v, 0,11 ± 0,023 nm at 35 % v/v and 0,10 ± 0,023 nm at 50 % v/v in DMSO/water mixtures. The low RMSD values observed across all solvent systems suggest that β-CD maintains a relatively rigid structure, a property that may contribute to its selective complexation mechanism.

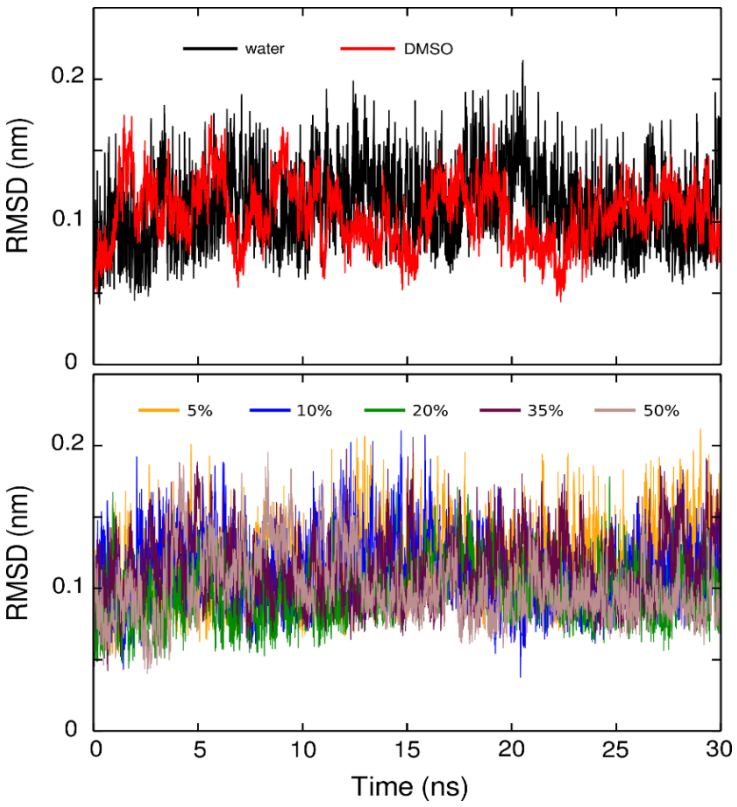


Figure II.1.2. Variation in the RMSD of β-CD atoms over 30 ns of MD simulation in pure water (black), pure DMSO (red), and DMSO/H_2O mixtures containing different DMSO concentrations: 5% (yellow), 10% (blue), 20% (green), 35% (purple), and 50% (pink).

To investigate the local structural changes induced by the solvent type, the root-mean-square fluctuation (RMSF) values were calculated for each atom of the α-D-glucose units. The results, averaged over the seven glucosidic subunits, are presented in **Figure II.1.3**, which also illustrates the atom nomenclature of the glucopyranose monomer. RMSF calculations were performed only for the two extreme solvent conditions, namely pure water and pure DMSO.

The RMSF values of individual β-CD atoms were lower in DMSO than in water, although similar fluctuation patterns were observed in both solvents. No significant differences were observed for most CD atoms, indicating that the fluctuations of the glucopyranose monomer are largely independent of the solvent type. However, increased fluctuations were observed in the peripheral groups, particularly the hydroxyl groups at positions 2 and 3, with the most pronounced fluctuations occurring at position 6 in both water and DMSO. These fluctuations are likely associated with interactions involving the solvent/cosolvent, such as the formation of intermolecular hydrogen bonds, as well as the mobility of the hydroxyl group attached to the C^6 outside the glucopyranosic ring. The RMSF values observed at positions 2, 3, and 6 indicate increased local flexibility in these regions, consistent with the dynamic mobility of hydroxyl groups, which are commonly associated with solvent-exposed or conformationally adaptable sites. The higher RMSF values of the hydroxyl group at position 6 reflect the flexibility of the -CH_2-OH groups located at the primary rim of β-CD, which may influence how PCZH-NO_3 accesses the cyclodextrin cavity through its narrower opening.

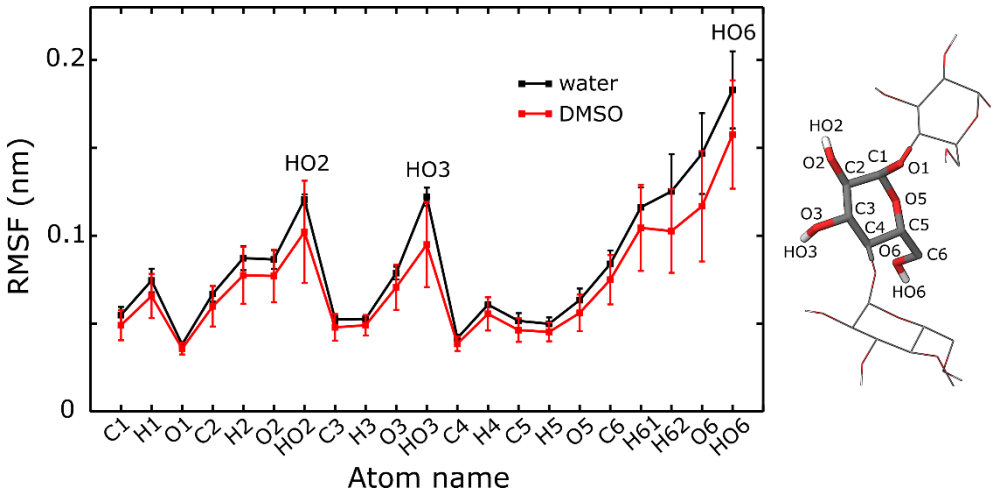


Figure II.1.3. RMSF variations for individual atomic positions in β-CD, calculated from simulations performed in pure solvents (water and DMSO).

The next stage of the analysis focused on investigating the differences in affinity of DMSO and water molecules for the β-CD cavity, as reflected by the residence times of DMSO molecules within the β-CD cavity, which are inversely proportional to the average exchange rate (ns^{-1}) of DMSO molecules acting as guest species within the cavity.

Figure II.1.4 shows that individual DMSO molecules dynamically enter and leave the β-CD cavity. Quantitative analysis revealed that, at 5% v/v DMSO, individual DMSO molecules exhibited an average exchange rate of 0.19 ns^{-1} within the β-CD cavity. This exchange rate increased to 0.27 ns^{-1} at 50% v/v DMSO, indicating shorter residence times per molecule due to the greater number of competing DMSO molecules. The cavity remained predominantly occupied throughout the simulations, and the time intervals during which it was not occupied by DMSO consistently corresponded to the presence of water molecules. This pattern suggests reciprocal substitution processes involving DMSO molecules within the cavity, highlighting dynamic competition between the two solvents, with DMSO exhibiting a clear preferential binding behavior under all investigated solvent conditions. Due to the dynamic nature of the system, DMSO molecules tend to remain within the β-CD cavity through continuous molecular exchange, whereas water molecules preferentially interact with the exterior of the β-CD host through hydrogen bonding with its free hydroxyl groups. These findings suggest that DMSO exhibits a higher affinity for β-CD through inclusion complex formation. Consequently, PCZH-NO_3 and DMSO compete for inclusion within the β-CD cavity.

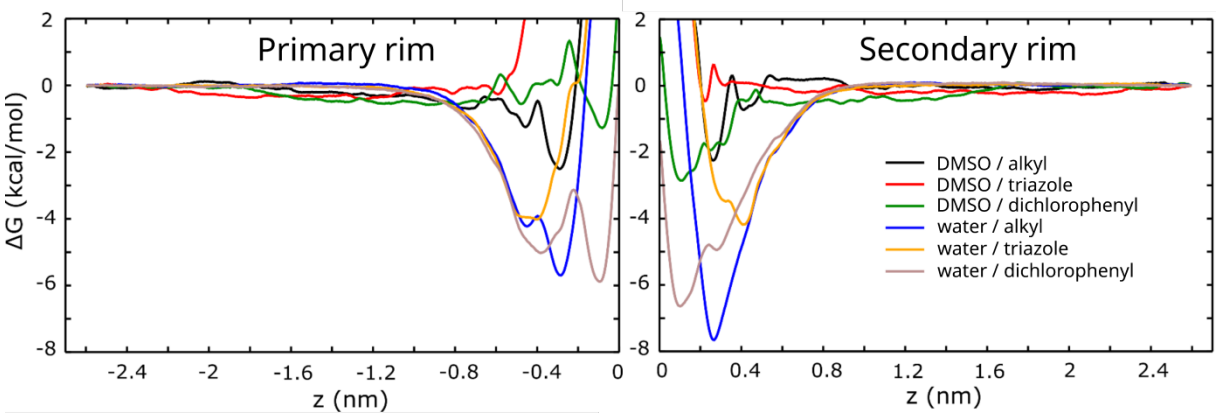


Figure II.1.6. Potential of mean force (PMF) profiles illustrating the influence of complexation geometry on the interaction between PCZH-NO_3 as the guest molecule and β-CD as the host molecule. The left panel shows complexation involving the insertion of PCZH-NO_3 through the narrower (primary) rim of β-CD, whereas the right panel shows complexation through the wider (secondary) rim, highlighting differences in binding affinity and complex stability.

For complexation through the primary rim, the binding affinity in DMSO follows the order: alkyl > dichlorophenyl > triazole, whereas in water, the order is dichlorophenyl ~ alkyl > triazole. The complexation process through the primary rim in DMSO exhibits behavior similar to that observed for complexation through the secondary rim in water. Likewise, a comparable trend is observed in water, where the binding affinity of PCZH-NO_3 at the primary rim resembles that determined for the secondary rim in DMSO. This suggests that the equilibrium complexation of PCZH-NO_3 in different binding modes is governed by interactions similar to those controlling complexation through the secondary rim. In the case of complexation through the primary rim, the hydroxyl groups involved in hydrogen bond formation are predominantly those located at position 6. Overall, the PMF profiles presented in **Figure II.1.6** indicate that the complexation of the guest molecule PCZH-NO_3 with CD is thermodynamically favorable for interactions through both the secondary and primary rims, with a higher binding affinity observed for the secondary rim.

To quantitatively evaluate the influence of the DMSO/H_2O (v/v) ratio on binding affinity, PMF profiles were constructed for the complexation process at different solvent compositions, ranging from 5% to 50% DMSO/H_2O (v/v). The results are presented in **Figure II.1.7-A**. For this analysis, a single molecular geometry was selected, corresponding to the most favorable binding mode through the wider rim in DMSO, in which the dichlorophenyl moiety is included within the β-CD cavity (**Figure II.1.6**). According to the PMF profiles presented in **Figure II.1.7-A**, the interaction between PCZH-NO_3 and CD is most favorable at 5% DMSO/H_2O (v/v), with a ΔG value of approximately -6.1 kcal/mol, and least favorable at 50% DMSO/H_2O (v/v), with a ΔG value of approximately -2.85 kcal/mol. These results indicate that DMSO, acting as a cosolvent, plays a significant role in the complexation process, progressively weakening the binding affinity as the DMSO/H_2O (v/v) ratio increases, as reflected by the increasingly less negative binding free energy.

Based on the PMF calculations presented in **Figures II.1.6** and **II.1.7-A**, an overall free energy profile for the complexation process as a function of the DMSO/water ratio was constructed, as shown in **Figure II.1.7-B**. The theoretical calculations indicate that complexation between PCZH-NO_3 and β-CD remains thermodynamically favorable in the presence of DMSO as a cosolvent, with only minor effects at low concentrations of up to 10% DMSO/H_2O (v/v). However, at concentrations exceeding 50% DMSO/H_2O (v/v), complex formation is likely to be inhibited, as DMSO reduces the magnitude of the complexation free energy to approximately -3 kcal/mol.

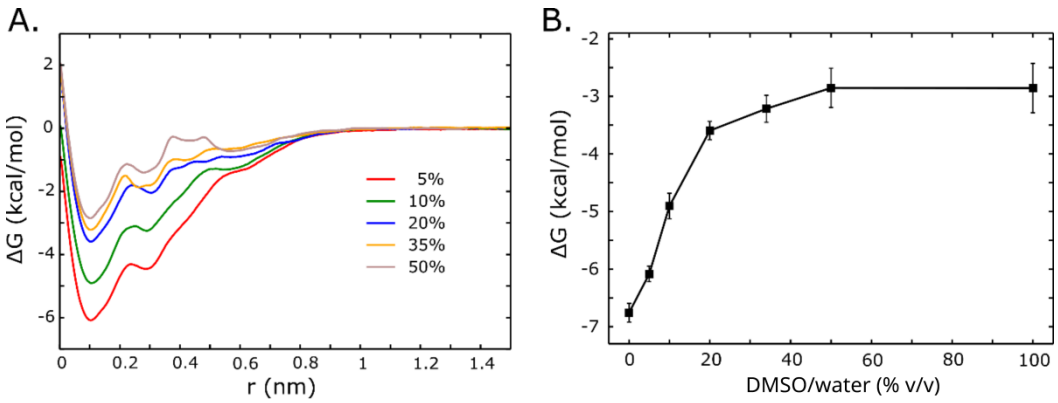


Figure II.1.7. Representation of: A. Gibbs free energy profiles for the PCZH-NO_3/CD complex in different DMSO/H_2O mixtures (5-50%) and B. relative Gibbs free energies of complexation at different DMSO/H_2O ratios.

The formation of the complex in the investigated solvents was monitored by changes in the chemical shifts of specific protons in both the host and guest molecules. Upon formation of the inclusion complex, the internal protons of CD (H-3' and H-5') exhibit upfield chemical shifts due to magnetic anisotropy effects induced by the included guest molecule. In this case, the formation of inclusion complexes was further confirmed by changes in the chemical shifts of the aromatic protons of PCZH-NO_3.

The ^{1}H NMR spectrum of free/non-complexed PCZH-NO_3 (**Figure II.1.8-B**) reveals signals corresponding to two diastereoisomers, consistent with previously reported data, in a 1:2 ratio determined from signal integration.

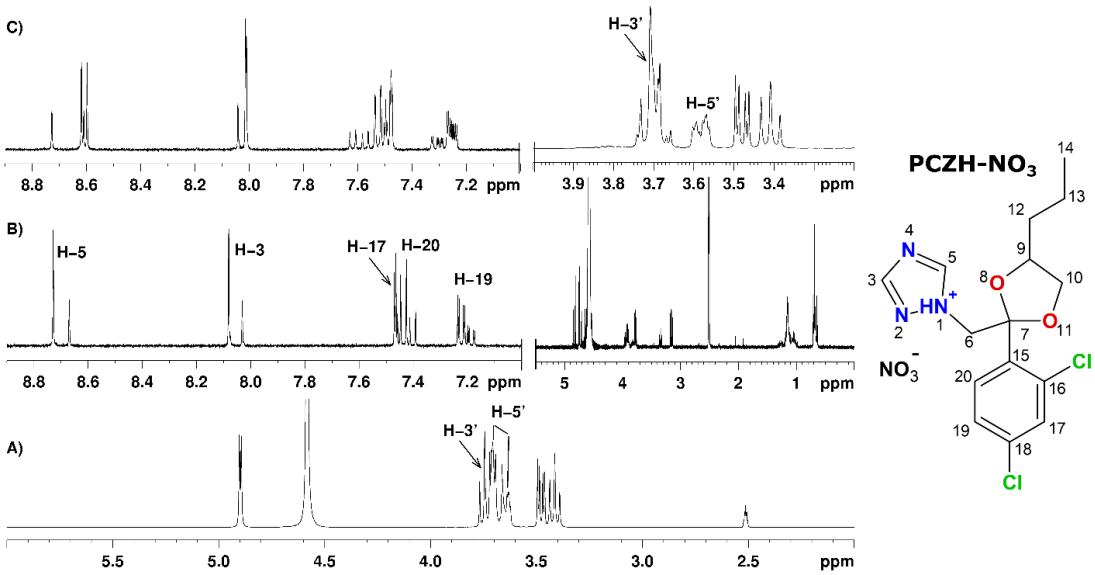


Figure II.1.8. ^{1}H-NMR spectra of β-CD (A), PCZH-NO_3 (B) and the inclusion complex β-CD/PCZH-NO_3 (C), record in 95:5 (v:v) mixture between D_2O:DMSO, together with the chemical structure of PCZH-NO_3 (right side).

The spectra presented in **Figure II.1.8** reveal changes in the resonance frequencies of the internal H-3' and H-5' protons of β-CD, as well as the aromatic protons of the triazole ring (H-3 and H-5) and the 2,4-dichlorophenyl ring (H-17, H-19, and H-20) of PCZH-NO_3, depending on the solvent composition. Changes in the chemical shifts of the aliphatic protons of PCZH-NO_3 could not be monitored due to the complex multiplicity of the signals arising from scalar couplings. As shown, the chemical shift differences depend on the percentage of DMSO added as a cosolvent. The chemical shift perturbation profiles as a function of DMSO percentage for the H-3 and H-5 protons of β-CD are presented in **Figure II.1.9**.

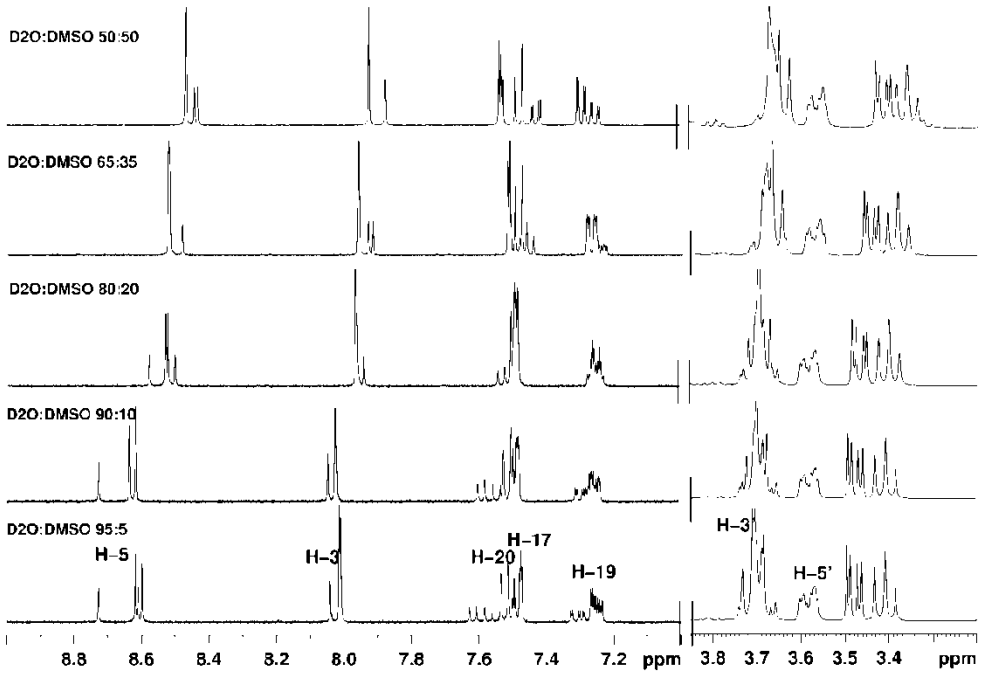


Figure II.1.9. ^{1}H-NMR spectra of the inclusion complex β-CD/ PCZH-NO_3 which shows the chemical shift variations and the spectral splittings dependent of the DMSO percentage.

II.1.4. Conclusions

This study provides a comprehensive analysis of the formation of inclusion complexes between β-cyclodextrin (β-CD) and PCZH-NO_3, a triazole derivative exhibiting antifungal activity, in different solvent environments by combining molecular dynamics (MD) simulations with nuclear magnetic resonance (NMR) spectroscopy. The results highlight the crucial role of solvent composition, demonstrating that DMSO exhibits a pronounced preference for interacting with the β-CD cavity compared to water, even at low DMSO/water ratios. The findings reveal that DMSO competes with both water and the drug molecule for

occupancy of the β-CD cavity, while MD simulations enabled a detailed investigation of these competitive interactions. The theoretical results demonstrate that inclusion complex formation is significantly influenced by solvent composition, with DMSO preferentially occupying the β-CD cavity.

The RMSF and RDF analyses revealed that hydrophobic interactions and hydrogen bonding are the primary factors governing the stabilization of these complexes. Furthermore, potential of mean force (PMF) calculations provided additional evidence of the energetically favorable nature of complexation, particularly in solvent mixtures containing low concentrations of DMSO, where the highest binding affinities were observed. The ^{1}H NMR and ROESY spectra provided experimental validation, revealing changes in chemical shifts and chiral discrimination within the inclusion complexes. These experimental observations are in good agreement with the theoretical predictions, further supporting the role of dynamic solvent interactions in controlling the complexation process.

The findings provide a deeper understanding of cosolvation effects arising from the competition between DMSO and water during the inclusion of PCZH-NO_3 within the β-CD cavity, offering atomistic insights into the mechanisms governing host-guest dynamics. Overall, these results provide valuable insights into the formation of cyclodextrin inclusion complexes in mixed-solvent environments, with important implications for their application in drug delivery systems designed for poorly water-soluble compounds. The conclusions emphasize the importance of solvent composition in optimizing cyclodextrin-based formulations according to the physicochemical properties of the target guest molecule (drug).

II. 2. 2,6-DIAMINO-1-N-HYDROXY-4-(PYRROLIDIN-1'-YL)PYRIMIDIN-1-IUM L-2-OXOTHIAZOLINE-4-CARBOXYLATE (MPPC)/β-CD INCLUSION COMPLEXES: THE ROLE OF ORGANIC IONS

The study on Minoxicapil aimed to improve the properties of MPPC, the active ingredient used to stimulate hair growth and treat alopecia (Tirnovan, et al., 2026). The research was motivated by the low aqueous solubility of MPPC and the risk of irritation associated with the use of ethanol or surfactants in topical formulations. To overcome these limitations, the formation of an inclusion complex between MPPC and β-cyclodextrin (β-CD) was investigated.

The **scope of the study** was to determine the selectivity, stability, and nature of the intermolecular interactions involved in the complexation of MPPC with β-cyclodextrin, with particular emphasis on the distinct roles of the cation and anion. To identify the included species and its preferred orientation, complementary methods involving molecular docking, molecular dynamics simulations, free energy calculations, and nuclear magnetic resonance (NMR) spectroscopy were employed.

The **original contribution** lies in elucidating the mechanism underlying the selective complexation of the cationic component of MPPC and characterizing the interactions that stabilize the host–guest association. Correlating the theoretical results with NMR data enabled the identification of a partial inclusion mode, in which the pyrrolidine moiety penetrates the hydrophobic cavity of β-cyclodextrin, while the pyrimidine moiety remains exposed to the surrounding environment. The anion does not form a stable inclusion complex under the investigated conditions.

The **results** obtained support the formation of a 1:1 inclusion complex, with a preference for the direct orientation of the cation. The association exhibits moderate stability and reversible behavior, stabilized by hydrophobic interactions and hydrogen bonding. Under the investigated experimental conditions, both free MPPC and the MPPC/β-cyclodextrin complex exhibited favorable biocompatibility. Furthermore, complexation promoted the proliferation of human hair follicle dermal papilla cells at lower MPPC concentrations than those required for the free compound. These findings provide a mechanistic and experimental basis for employing β-cyclodextrin complexation as a strategy to optimize pharmaceutical formulations containing ionic active pharmaceutical ingredients.

II.2.3. Results and Discussions

II.2.3.1. Theoretical Results and Discussions

Molecular docking studies

The molecular docking study revealed that the most stable binding mode occurs when the pyrrolidine ring interacts with the wider, secondary rim of β-CD. In this configuration, the cation (2,6-diamino-1-hydroxy-4-(pyrrolidin-1-yl)pyrimidinium) adopts a direct orientation, with the hydrophobic pyrrolidine ring located inside the cavity and the more hydrophilic pyrimidine ring positioned outside (**Figure II.2.2-a/d**). In the system shown in **Figure II.2.2-f**, the most favorable structure corresponds to a 2:2 complex (two cations and two β-CD molecules), which nevertheless maintains an overall effective stoichiometry of 1:1.

The effect of the anion on complexation was also evaluated through binding energy calculations. No significant differences were observed between anion-β-CD complexation and the association of the anion with cations already included within β-CD (**Figure II.2.2-b-i**). The docking poses indicate that the protons of the hydrophobic ring are located in close proximity to the H-3 and H-5 protons within the β-CD cavity. Furthermore, the NH_2 groups interact with the secondary hydroxyl groups at the wider rim of β-CD (**Figure II.2.2-a/c-g**).

For inclusion complexes containing both the cation and the anion (L-2-oxothiazolidine-4-carboxylate), the ions form a stacked ion-pair arrangement, in which the cation is included within the β-CD cavity while the anion remains outside (**Figure II.2.2-c/d**).

Among the simulated systems, the cation-β-CD complex exhibits the lowest interaction energy, whereas the anion-β-CD complex exhibits the highest. These findings indicate that the cation-β-CD system is more stable than the anion-β-CD complex.

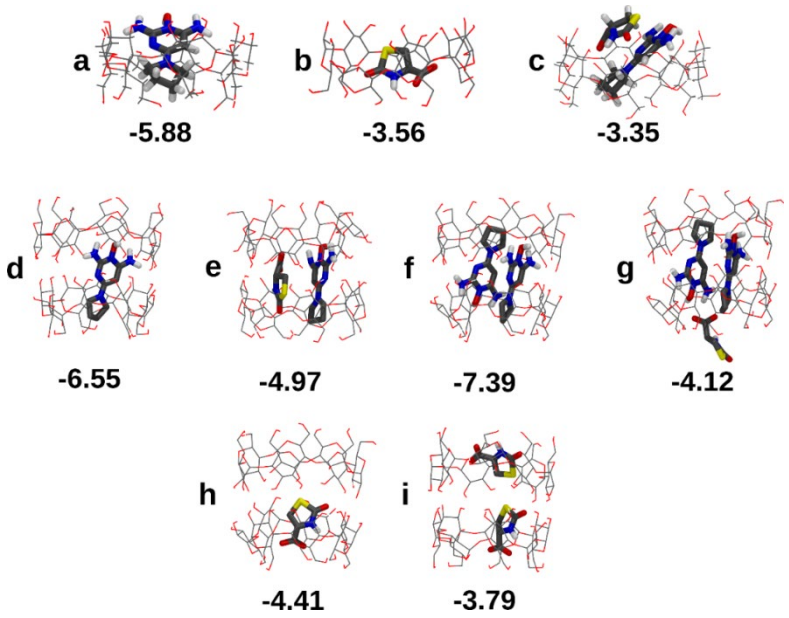


Figure II.2.2. Graphical representation of the MPPC-β-CD complex in different configurations obtained from molecular docking calculations: (a) cation-β-CD (1:1), (b) anion-β-CD (1:1), (c) anion + cation-β-CD (1:1), (d) cation-β-CD (1:2), (e) anion + cation-β-CD (1:2), (f) cation-β-CD (2:2), (g) anion + cation-β-CD (2:2), (h) anion-β-CD (1:2), and (i) anion-β-CD (2:2). Binding energies are expressed in kcal/mol.

Molecular Dynamics

In the MD simulation performed in the presence of both ions, the anion was observed to enter the β-CD cavity more rapidly than the cation due to its smaller size. The anion remained within the cavity until approximately 700 ns, when an exchange between the two ions occurred, after which the cation remained inside the cavity for the remainder of the simulation, up to 2000 ns (**Figure II.2.6**). Compared to the previous simulation (performed with Cl^- anions), no further exchange of cations within the β-CD cavity was observed, suggesting that the anion promotes the formation of a more stable inclusion complex.

At the same time, a free aggregate involving the other molecules in the system was formed (**Figure II.2.7**), predominantly located near the wider, secondary rim of the β-CD cavity. This observation is consistent with the lower aqueous solubility observed experimentally and with the molecular arrangement predicted by docking calculations (**Figure II.2.2-c/d**). The formation of this aggregate accounts for the slower inclusion of the cation into the β-CD cavity during the simulation and exhibits a less transient character compared to the molecular arrangements shown in **Figure II.2.5**.

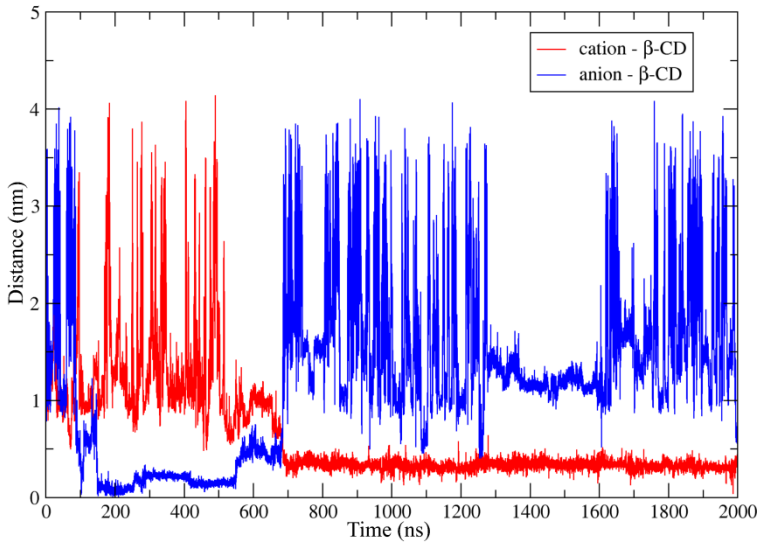
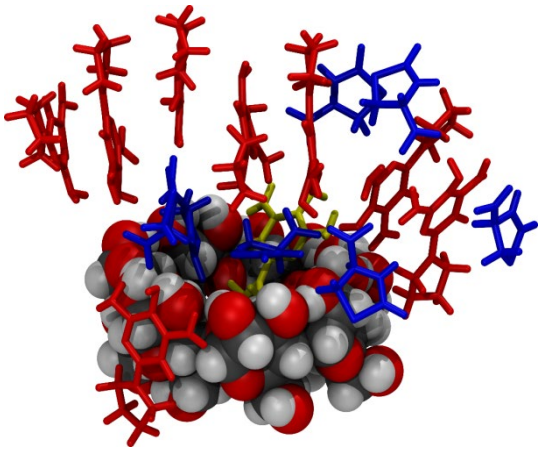


Figure II.2.6. Distance profiles between the MPPC cation and anion and β-CD over the course of a 2000 ns molecular dynamics simulation.

Figure II.2.7. Representation of the aggregated system at the end of the MD simulation, highlighting its structural features. Color coding: MPPC cations - red; MPPC anions - blue; cation included within the β-CD cavity - yellow. The van der Waals surface of β-CD is shown in its default atomic colors.



Umbrella sampling method

The results obtained from umbrella sampling simulations show that the free energy minimum is lower when the MPPC cation adopts a direct orientation within β-CD, with the pyrrolidine moiety located inside the CD cavity and the pyrimidine ring oriented toward the wider, secondary rim (**Figure II.2.12-a**), compared to the reverse orientation (**Figure II.2.12-b**). This finding indicates that complexation of the cation is more favorable in the direct orientation than in the reverse orientation.

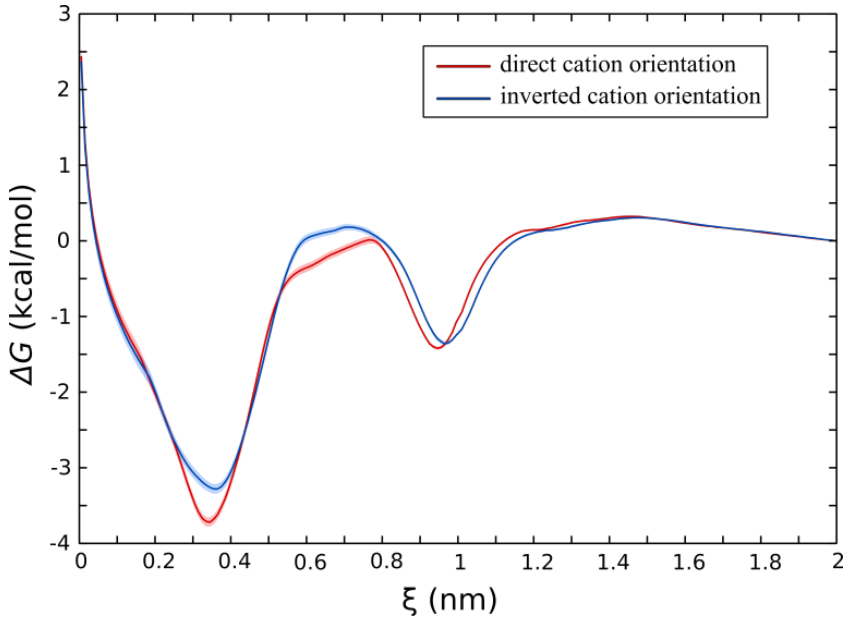


Figure II.2.11. Potential of mean force (PMF) profiles, with standard deviations represented by shaded regions, for the MPPC cation interacting with β-CD in direct and reverse orientations.

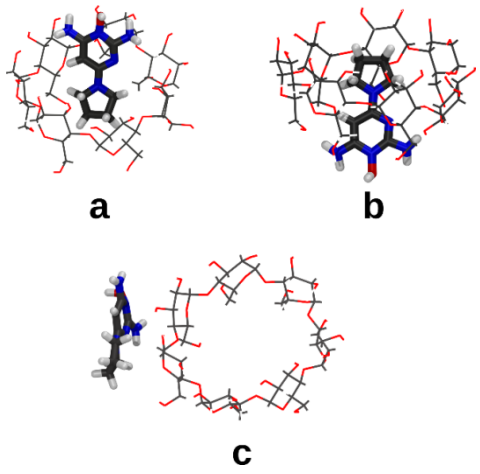


Figure II.2.12. Structures of the β-CD/MPPC inclusion complexes corresponding to the free energy minima (ΔG) obtained from PMF calculations.

The direct orientation of the MPPC cation exhibits a lower free energy minimum (ΔG ~ -3.72 kcal/mol) at ξ ~ 0.32 nm (**Figure II.2.11** and **Figure II.2.12-a**) compared to the reverse orientation (ΔG ~ -3.28 kcal/mol), illustrated in Figure II.2.11 and by the complex shown in **Figure II.2.12-b**. This result indicates that the direct orientation, in which the pyrrolidine ring is located inside the cavity and the pyrimidine ring is oriented toward the wider, secondary rim, is energetically more favorable. An additional secondary free energy minimum is observed at ξ ~ 1 nm, with similar values for both PMF profiles (ΔG ~ -1.4

kcal/mol). This minimum corresponds to a configuration in which the MPPC cation is located near the external surface of β-CD (**Figure II.2.12-c**), as also observed in the MD simulations. The free energy of this state is relatively close to that of the primary minimum in the reverse orientation, further reducing the preference of the cation for the reverse inclusion geometry due to competition between the accessible states.

Furthermore, intermolecular interactions between the β-CD hydroxyl groups (β-CD-OH) and the MPPC amino groups (MPPC-NH_2) contribute to the stabilization of the direct orientation of the MPPC cation within β-CD (**Figure II.2.12-a**). Conversely, the size of the pyrimidine ring, together with its two attached NH_2 groups, results in pronounced steric hindrance upon interaction with the primary hydroxyl groups at the narrower rim of β-CD. This explains the lower stability of the MPPC cation in the reverse orientation (**Figure II.2.12-b**), as well as the reduced probability of this configuration occurring in the system, since the entry of the cation into the β-CD cavity is sterically hindered in this orientation.

In both configurations (a) and (b) (**Figure II.2.12**), the MPPC cation does not fully penetrate the β-CD cavity. Only the pyrrolidine ring, containing hydrophobic sp^3-hybridized carbon atoms, is included within the cavity, where it establishes weak van der Waals interactions with the H-3 and H-5 protons. The more hydrophilic pyrimidine ring remains oriented toward the exterior of β-CD, where it interacts with the surrounding solvent and with the primary or secondary hydroxyl groups through hydrogen bonding.

II.2.3.2. Experimental Results and Discussions

Nuclear magnetic resonance (NMR) spectroscopy was employed as the primary analytical technique to investigate the structural characteristics of the MPPC formulation and to confirm its interaction with β-CD. All NMR experiments were conducted under controlled temperature conditions using standard one- and two-dimensional homo- and heteronuclear correlation techniques, enabling the unambiguous assignment of spectral signals and the identification of host-guest interactions. Particular attention was paid to solvent composition and experimental conditions to preserve labile functional groups and ensure spectral reproducibility. Specifically, rotating-frame Overhauser effect spectroscopy (ROESY) experiments were performed to identify spatial proximities between the β-CD cavity and the MPPC cation, providing direct evidence of inclusion complex formation.

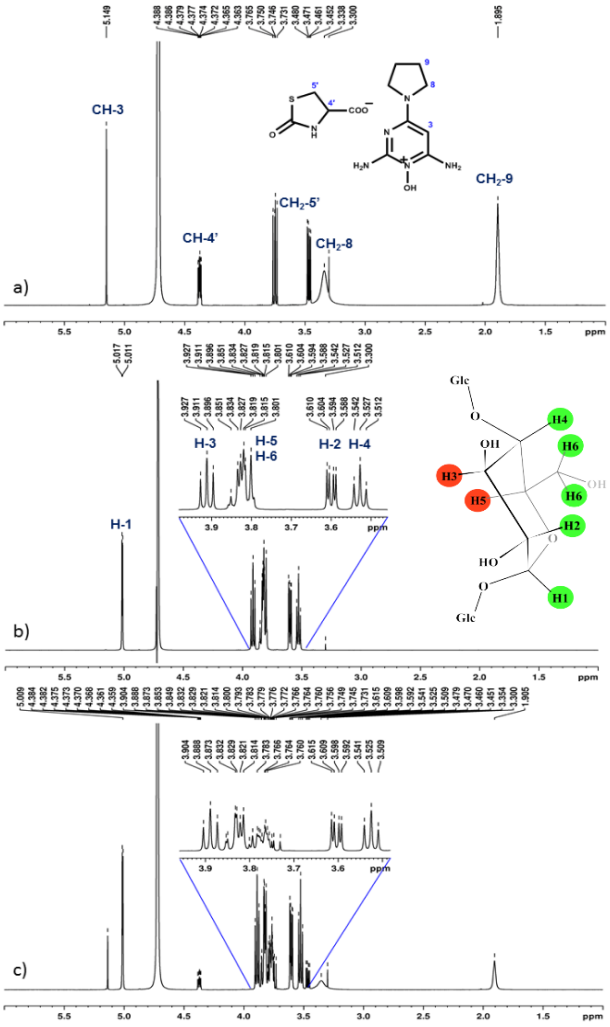


Figure II.2.14. ^{1}H NMR spectra recorded with suppression of the residual water signal for (a) the native MPPC formulation, (b) β-CD, and (c) the MPPC-β-CD mixture. All spectra were acquired under identical experimental conditions at a frequency of 600 MHz.

The second parameter used to evaluate the extent of intermolecular binding between MPPC and β-CD was the association constant (K_a). This parameter can be determined by ^{1}H NMR titration using a different set of solutions and a distinct analytical approach compared to the continuous variation method. Aqueous stock solutions (90% H_2O and 10% D_2O) of β-CD (15 mM) and MPPC (300 mM) were prepared and subsequently used to obtain 13 samples with varying β-CD concentrations (0-15 mM). The MPPC concentration was maintained constant at 3 mM throughout the entire sample series. The ^{1}H NMR spectra were recorded under identical experimental conditions, with suppression of the dominant water signal, and the chemical shift changes across the 13 samples were monitored. The association constant was determined using the NMR-adapted Benesi-Hildebrand equation (Fielding, 2000), by monitoring the chemical shift variations of the CH_2-9 protons of the MPPC cation:

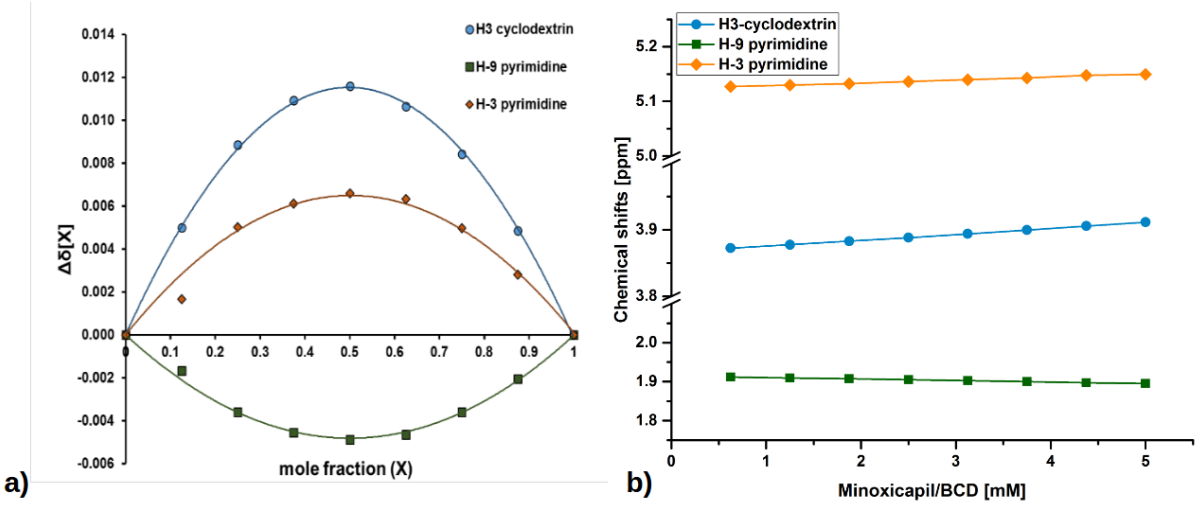


Figure II.2.18. (a) Job plots obtained from NMR titrations, indicating a 1:1 stoichiometry for the β-CD/MPPC complex. Three proton signals were monitored: H-3 of β-CD and H-3 and H-9 of the pyrimidine moiety. (b) Chemical shift variations as a function of MPPC or β-CD concentration for the monitored protons, used to construct the Job plots.

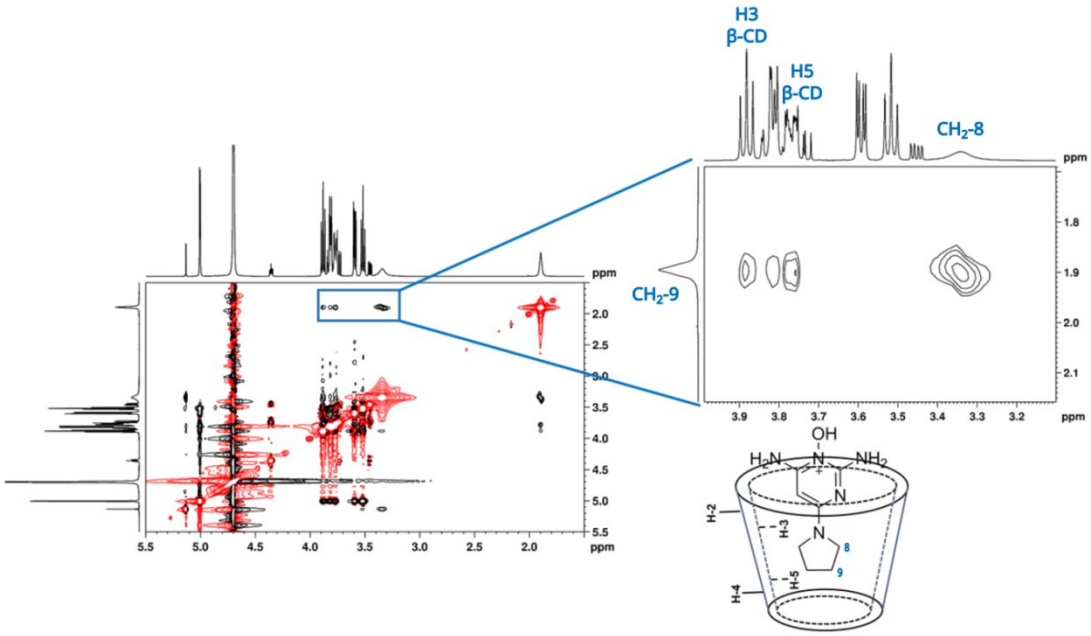


Figure II.2.20. Two-dimensional ^{1}H-^{1}H ROESY spectrum of the β-CD-MPPC mixture at a 1:1 molar ratio, showing intermolecular NOE cross-peaks between the host and guest molecules. The proposed geometry of the MPPC cation within the β-CD cavity in solution is illustrated in the bottom-right corner.

II.2.4. Conclusions

The combined interpretation of the theoretical results and NMR data leads to the same conclusion. The MPPC cation is the species partially included within the host-guest complex, with its pyrrolidine ring oriented toward the interior of the hydrophobic β-CD cavity, whereas the anion does not exhibit stable inclusion due to its high mobility in solution and smaller molecular volume. Umbrella sampling calculations demonstrate that the direct orientation is energetically more favorable, with the primary PMF minimum located at approximately -3.72 kcal/mol.

The Job plots obtained from NMR titrations revealed the formation of a 1:1 inclusion complex between β-CD and the MPPC cation, with an association constant of K_a = 76 M^{-1} (corresponding to a binding free energy of approximately -2.57 kcal/mol). This value is characteristic of a moderately stable and reversible host-guest system and is relatively close to the theoretically determined PMF value.

Under the experimental conditions investigated, both free and complexed MPPC exhibited limited permeation into the receptor compartment in Strat-M® diffusion studies and favorable in vitro biocompatibility with human hair follicle dermal papilla cells, as assessed using the EZ-Cytox WST-1 cell viability assay.

These findings establish the mechanistic and experimental basis for MPPC-β-CD complexation and support further investigation of this system for the development of topical formulations. Future research should focus on substituted cyclodextrins with enhanced binding affinity, in vivo validation of biological activity, and evaluation of controlled drug release in solvent systems that more closely resemble physiological conditions.

Taken together, the two studies demonstrate that the inclusion mechanism in β-cyclodextrin is governed by both the composition of the reaction medium and the structural and ionic characteristics of the guest molecule. The contribution of **Chapter II** lies in elucidating two complementary mechanisms: cosolvent-guest competition for occupancy of the cyclodextrin cavity and the selective inclusion of one component of an ionic formulation. These findings highlight the importance of explicitly considering the solvent and all species present in the system when optimizing inclusion complexes for pharmaceutical applications.

CHAPTER III. MOLECULAR SYSTEMS WITH POTENTIAL APPLICATIONS IN DRUG DELIVERY: IN SILICO STUDIES ON THE INFLUENCE OF THE SOLVATION MODEL ON THE LOWER CRITICAL SOLUTION TEMPERATURE (LCST) OF PNIPAM-BASED STIMULI-RESPONSIVE POLYMERS

The study investigated the thermoresponsive behavior of poly(N-isopropylacrylamide) (PNIPAM), a polymer with potential applications in drug delivery and controlled drug release. PNIPAM exhibits a lower critical solution temperature (LCST), near which it undergoes a conformational transition from an extended to a compact state.

The **scope of the research** was to identify simulation conditions capable of reproducing as accurately as possible the experimentally observed conformational transition of PNIPAM near its lower critical solution temperature (LCST). Molecular dynamics simulations were performed to compare systems containing one and ten polymer chains, using the TIP3P, SPC/E, and TIP4P-Ew water models. The analysis focused on the influence of these parameters on hydration, polymer collapse, and the evolution of hydrogen bonding as a function of temperature.

The **original contribution** lies in characterizing the distinct effects of the water model and the number of polymer chains on the description of the conformational transition. The study highlights the role of interchain interactions in stabilizing compact conformations and identifies bridging hydrogen bonds as the most sensitive descriptor of the transition among those investigated.

The **results** obtained demonstrate that both types of systems qualitatively reproduce the thermoresponsive behavior of PNIPAM. However, the ten-chain system reaches equilibrium more rapidly and exhibits more stable compact conformations. Interchain interactions promote the formation of a denser structure with reduced water accessibility, while bridging hydrogen bonds undergo pronounced changes near the LCST. Among the investigated conditions, the combination of the ten-chain system and the TIP4P-Ew water model provides the clearest description of the transition, occurring at approximately 305 K. These findings provide methodological guidance for selecting appropriate simulation conditions for PNIPAM systems and establish a foundation for investigating functionalized structures or systems incorporating active pharmaceutical ingredients, with potential applications in controlled drug delivery.

III.3. Results and Discussions

The soluble-to-insoluble transition of PNIPAM, accompanied by an extended-to-collapsed conformational transition, was investigated using the following descriptors: radius of gyration (R_g), hydrogen bonding interactions, including polymer-water, polymer-polymer, and bridging hydrogen bonds, and the number of water molecules within the first hydration shell of the polymer. The LCST was identified as the temperature corresponding to the most pronounced inflection point or discontinuity in the temperature dependence of these descriptors.

The time series reveal fluctuations that increase in amplitude from 210 K to 305 K and become more frequent between 305 K and 400 K, with the exception of the SPC/E water model (**Figure III.5**). These fluctuations are most likely associated with thermal motion, which intensifies with increasing temperature and counteracts the collective interactions responsible for polymer collapse. The radius of gyration exhibits its highest values, with relatively small fluctuations, at 210 K, indicating stable, extended conformations. At 305 K and 400 K, R_g fluctuates considerably between approximately 18 Å and 8 Å, with the latter value corresponding to the collapsed state. This behavior suggests microscopic reversibility of polymer collapse, characterized by repeated transitions between extended and collapsed conformations.

Despite these fluctuations, PNIPAM exhibits an overall tendency toward a collapsed state, as demonstrated by the decrease in average Rg values with increasing temperature (**Figure III.6**). As the temperature increases from 210 K to 305 K, PNIPAM solvated using the TIP4P-Ew water model exhibits the greatest degree of collapse. Upon further heating to 400 K (95 K above the LCST), the polymer remains relatively stable in its collapsed state, whereas PNIPAM systems solvated using the TIP3P and SPC/E water models continue to undergo further collapse.

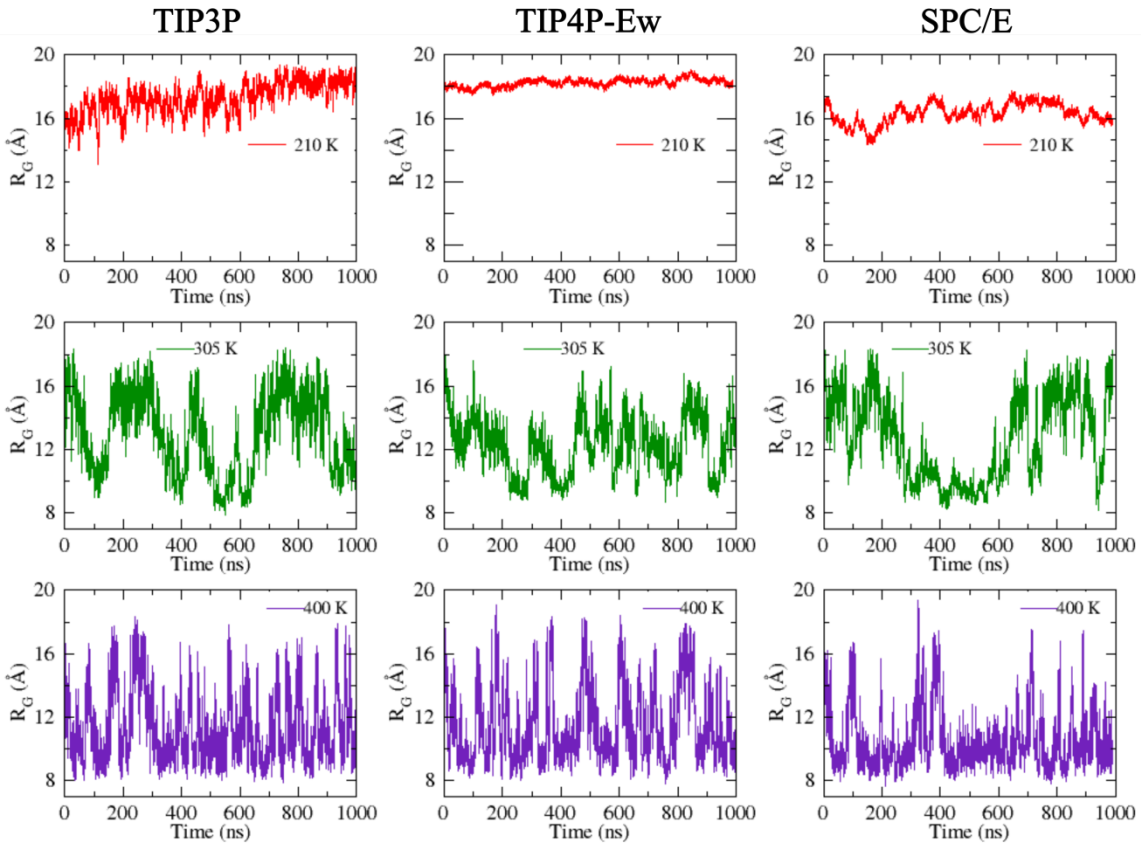


Figure III.5. Radius of gyration (R_g) for a single chain PNIPAM, over the entire simulation time of 1000 ns.

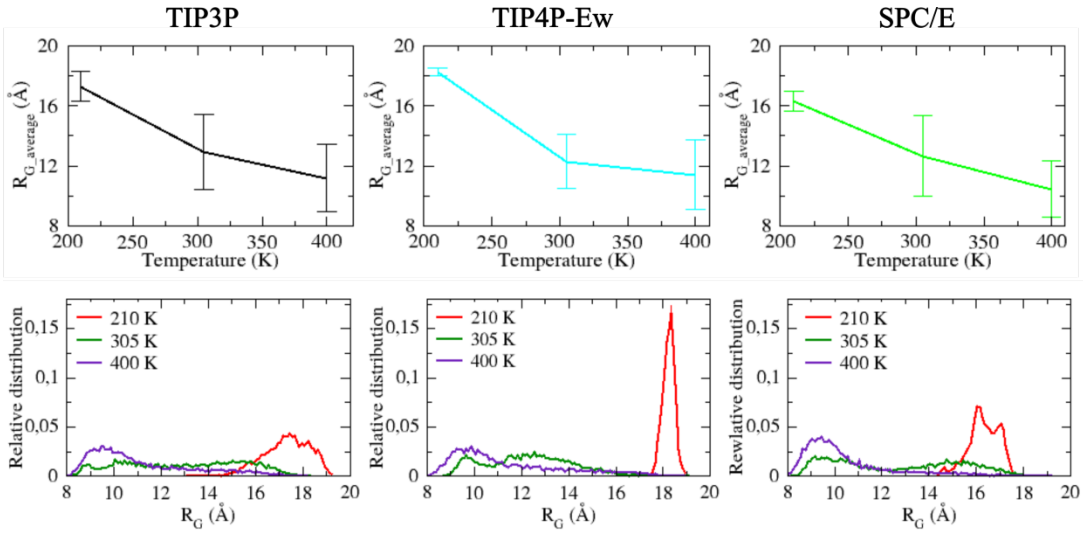


Figure III.6. Temperature dependence of the average radius of gyration (first row) and its relative distributions (second row) for a single PNIPAM chain over the entire 1000 ns simulation.

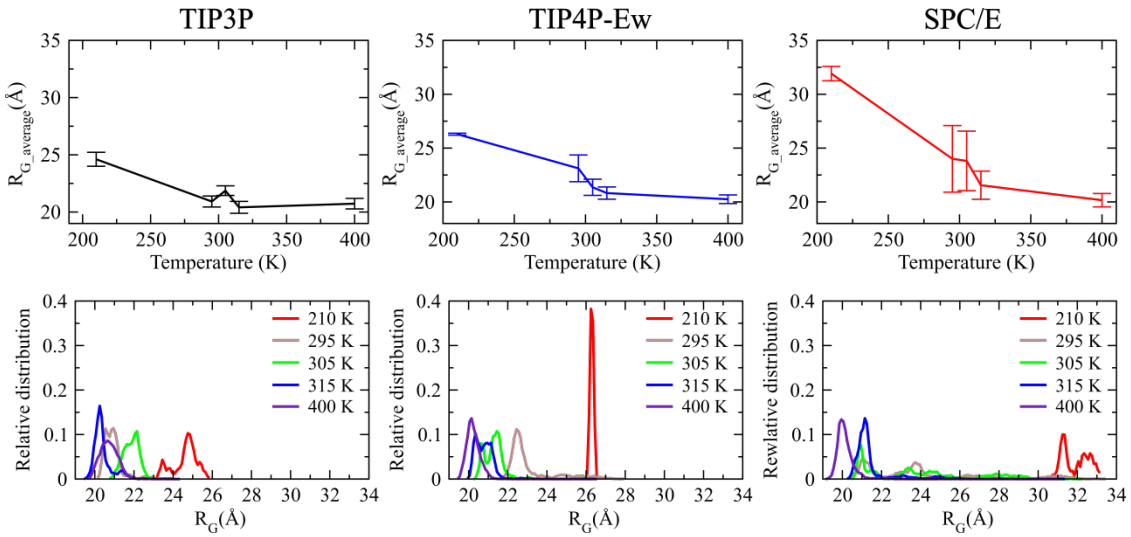


Figure III.10. Temperature dependence of the average radius of gyration (first row) and its relative distributions (second row) for ten PNIPAM chains over the entire 1000 ns simulation.

For all water models, the average Rg decreases with increasing temperature, indicating an overall tendency toward compaction. The influence of the water models is reflected in the degree of polymer compaction (25% for SPC/E, ~18% for TIP4P-Ew, and ~11% for TIP3P) and in the behavior of the system near the transition temperature. The TIP3P model produces noticeable discontinuities, followed by a slight increase in Rg up to 400 K, which is attributed to pronounced thermal fluctuations that are not sufficiently dampened by TIP3P.

The TIP4P-Ew and SPC/E models exhibit the most pronounced discontinuities at 305 K and 295 K, respectively. Beyond these temperatures, R_g reaches a plateau in the TIP4P-Ew system, indicating a stable compact state up to 400 K, whereas the SPC/E system exhibits slight additional compaction at higher temperatures. The relative distributions of the radius of gyration (**Figure III.10**), calculated using a bin width of 0.1 Å, further support these observations. The TIP4P-Ew model exhibits the narrowest and most pronounced peak at 210 K, reflecting a highly stable conformational state. At higher temperatures, TIP4P-Ew uniquely distinguishes the regime at 295 K from those at 305 K and above, while the overlapping distributions indicate the persistence of stable compact conformations. Collectively, these observations identify 305 K as the transition temperature.

Analysis of polymer-solvent hydrogen bonds

For the system containing ten PNIPAM chains, the number of polymer-water hydrogen bonds decreases with increasing temperature (**Figure III.15**). Minor differences are observed among the water models, primarily reflected in the number of polymer-polymer

hydrogen bonds and in the behavior beyond the transition temperature. The lowest number is obtained with the TIP3P water model, whereas the highest is observed with TIP4P-Ew, suggesting enhanced stability of the hydration shell above the transition temperature. These findings confirm that the number of polymer-water hydrogen bonds is only slightly influenced by the choice of water model, with the differences being primarily quantitative.

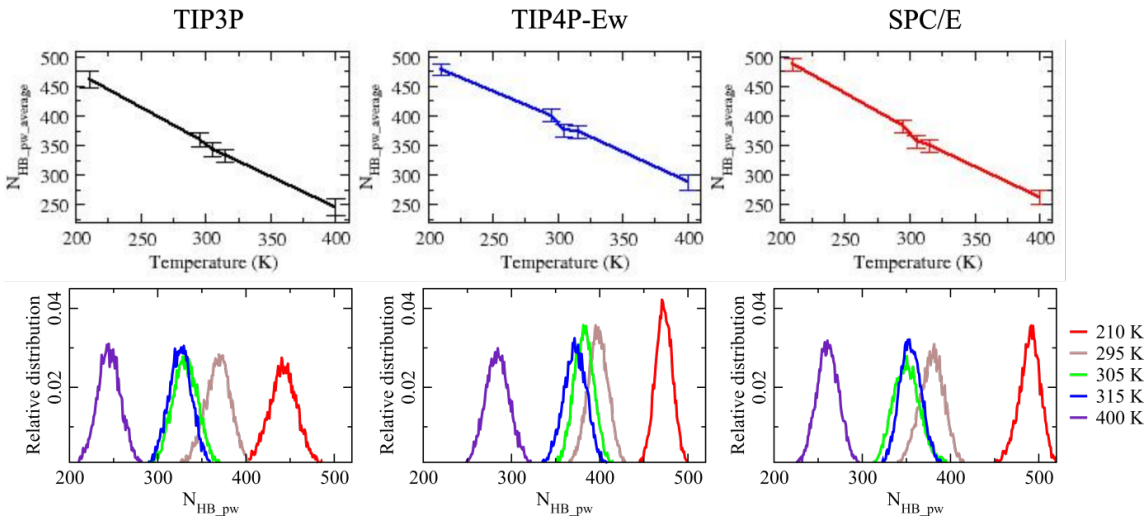


Figure III.15. Temperature dependence of the average number of polymer-water hydrogen bonds for ten PNIPAM chains over the entire simulation time.

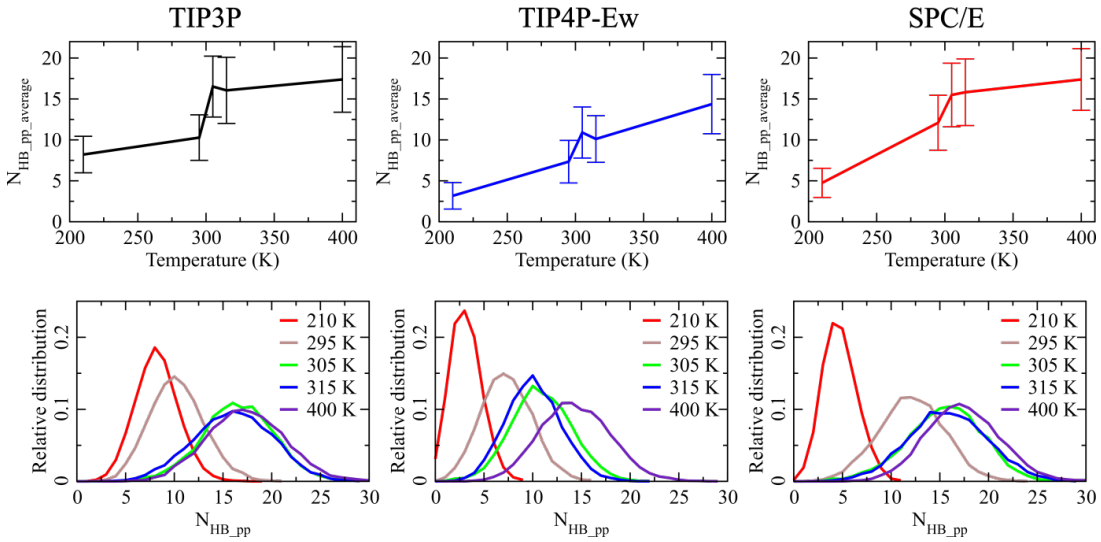


Figure III.19. Temperature dependence of the average number of polymer-polymer hydrogen bonds (first row) and their relative distributions (second row) for ten PNIPAM chains over the entire 1000 ns simulation.

For all water models, discontinuities are observed in the vicinity of the transition temperature, after which the TIP3P and SPC/E models exhibit an almost constant number of

polymer-polymer hydrogen bonds. In contrast, the TIP4P-Ew water model promotes the formation of additional polymer-polymer hydrogen bonds through more pronounced cooperative interactions between polymer chains, effectively counteracting the enhanced thermal fluctuations at elevated temperatures.

The increase in standard deviation with temperature reflects the transient nature of polymer-polymer hydrogen bonds. The relative distributions further support these observations: at 210 K, the distributions are centered around low hydrogen bond counts, whereas increasing temperature leads to broader distributions that progressively shift toward higher values, indicating the formation of an extensive but relatively unstable polymer-polymer hydrogen-bonding network.

Above 305 K, the distributions largely overlap, suggesting that once the transition temperature is exceeded, polymer-polymer hydrogen bonding becomes nearly insensitive to further increases in temperature.

III.4. Conclusions

The theoretical results demonstrate that both single-chain and multichain simulations reproduce the same qualitative thermoresponsive behavior of PNIPAM. However, only the system containing ten polymer chains captures a stable and realistic transition toward compact conformations, reaching equilibrium significantly faster than the single-chain system and highlighting the essential role of interchain hydrogen-bonding interactions.

The degree of polymer compaction is influenced by bridging hydrogen bonds, which can facilitate the proximity of polymer chains and promote interchain interactions, potentially leading to the formation of a denser polymer network with reduced water accessibility and partial dehydration. Among all the descriptors investigated, bridging hydrogen bonds proved to be the most sensitive indicator of the transition, exhibiting the most pronounced discontinuity near the LCST.

Although all water models reproduce the general collapse mechanism, TIP4P-Ew provides the most accurate description of the transition, correctly identifying the LCST at 305 K and producing a sharper and more consistent transition signal, particularly in the multichain system.

Therefore, within the framework of molecular dynamics simulations performed using the AMBER software package and the GAFF2 force field, the most accurate identification of the LCST for PNIPAM is achieved using systems containing ten PNIPAM chains, each consisting of 30 repeating units, solvated with the TIP4P-Ew water model. These conditions

require simulation times of approximately 600 ns to achieve adequate equilibration, while the most reliable results are obtained by analyzing only the final portion of the trajectory, corresponding to the equilibrium regime.

Overall, these theoretical findings provide a foundation for future investigations of PNIPAM-based systems incorporating active pharmaceutical compounds, as well as for the design of functionalized PNIPAM derivatives that could serve as drug delivery carriers.

CAPITOLUL IV. MOLECULAR SYSTEMS WITH POTENTIAL APPLICATIONS IN BIOIMAGING: A TD-DFT STUDY ON THE INFLUENCE OF MOLECULAR STRUCTURE ON THE ABSORPTION WAVELENGTH OF POLYCYCLIC AROMATIC HYDROCARBONS (PAHs) AND GRAPHENE QUANTUM DOTS (GQDs)

The study investigated the optical properties of polycyclic aromatic hydrocarbons (PAHs) and graphene quantum dots (GQDs), materials with potential applications in drug delivery and bioimaging (Li et al., 2019).

The **scope of the research** was to establish the relationship between molecular structure and the wavelengths of the absorption maxima of polycyclic aromatic hydrocarbons and graphene quantum dots (GQDs). This chapter complements the overall scope of the thesis by investigating the optical response of materials that could subsequently be explored for combining active pharmaceutical ingredient delivery with bioimaging capabilities. The study was motivated by the complexity of experimentally synthesized GQD materials, which makes molecular structure identification and spectral band assignment challenging (Langer et al., 2021). Using DFT and TD-DFT methods, structures containing between 18 and 316 atoms were investigated, including 23 polycyclic aromatic hydrocarbons and hexagonal GQD models with armchair and zigzag edges. Single-layer and multilayer configurations were compared, including pristine structures, structures functionalized with oxygen-containing groups, and structures incorporating structural defects.

The **original contribution** lies in the systematic and comparative characterization of the effects of molecular size, edge type, number of layers, functionalization, and structural defects on optical absorption properties. The analysis highlights the distinct responses of armchair- and zigzag-edged structures and enables the investigation of the combined effects of edge modifications and defects within the graphene plane.

The **results** obtained demonstrate that molecular size, number of layers, and edge type influence the electronic structure and the positions of absorption bands. Increasing the number of layers generally promotes a shift in absorption toward longer wavelengths, while functionalization with epoxy and carbonyl groups induces changes that depend on edge type and system configuration. The removal of two carbon atoms from the graphene plane produces some of the most pronounced bathochromic shifts observed among the investigated structures (Tirnovan, et al., 2026). These findings provide molecular-level insights into tuning the absorption properties of GQDs and identifying promising candidate structures for future bioimaging research. Evaluating their suitability for such applications requires further

investigation of their emission properties and behavior in biological environments, while their potential integration with the delivery and controlled release of active pharmaceutical ingredients remains a direction for future research.

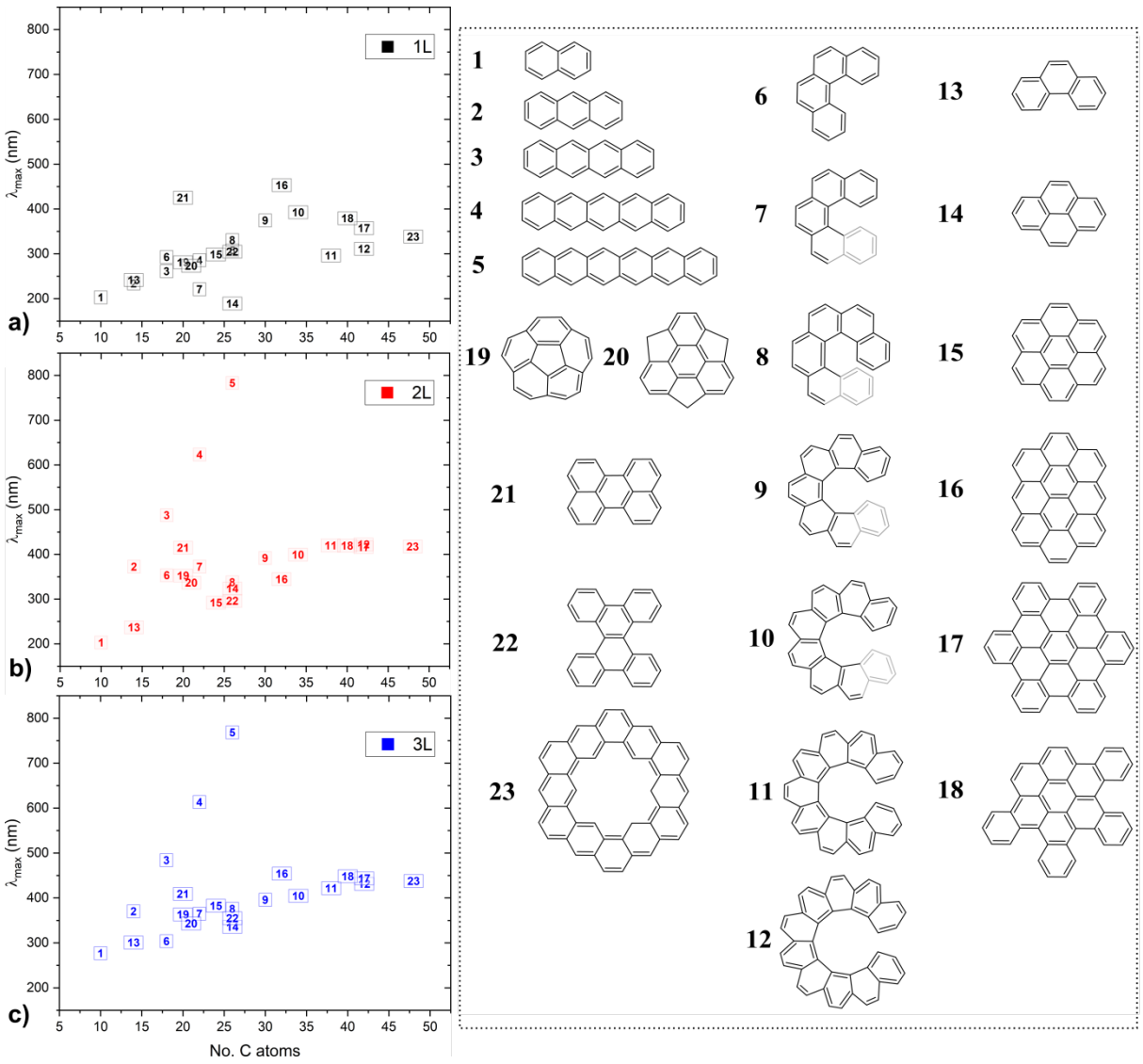


Figure IV.1. Graphical representation of the theoretically predicted maximum absorption wavelengths (λ_{max}) for PAH systems consisting of (a) one layer (1L), (b) two layers (2L), and (c) three layers (3L). (a) Molecular structures considered in this study: naphthalene-1, anthracene-2, tetracene-3, pentacene-4, hexacene-5, tetrahelicene-6, pentahelicene-7, hexahelicene-8, heptahelicene-9, octahelicene-10, nonahelicene-11, decahelicene-12, phenanthrene-13, pyrene-14, coronene-15, ovalene-16, hexabenzo[bc,ef,hi,kl,no,qr]coronene-17, tetrabenzo[a,d,g,j]coronene-18, corannulene-19, sumanene-20, perylene-21, dibenzo[g,p]chrysene-22, and kekulene-23. The absorption wavelength of pyrene-14 was excluded from the figure because λ_{max} < 200 nm.

The general trend indicates that as the size of the π-conjugated system increases, the absorption bands shift toward longer wavelengths. This effect is attributed to the gradual reduction in the energy gap between the excited states and the ground state, as reported in numerous previous studies, resulting from the increasing number of π-electrons involved in long-range conjugation within the graphene plane.

This trend is particularly pronounced in the linear acene family (naphthalene-1, anthracene-2, tetracene-3, pentacene-4, and hexacene-5), as well as in other molecular systems characterized by honeycomb-like aromatic structures, numbered 13-23. However, a plateau-like trend followed by a decrease is observed for compounds 17, 18, and 23. The presence of sp^3-hybridized carbon atoms in the sumanene structure (20) results in a maximum absorption wavelength of approximately 273 nm, located in the ultraviolet region.

The distorted molecular structures characteristic of the helicene family (6-12) lead to considerable variations in the maximum absorption wavelength, with oscillations depending on the number of aromatic units. The absorption maxima generally fall within the 200-400 nm range. A distinct behavior is observed for ovalene-16, which exhibits a maximum absorption wavelength of approximately 453 nm, corresponding to the blue region of the electromagnetic spectrum, in contrast to most other systems, which predominantly absorb in the UV region.

Clear differences can also be observed between the absorption wavelengths of isomeric structures that differ in the arrangement of their aromatic rings. These differences are strongly correlated with the extent of π-conjugation, as illustrated by the comparisons between structures 3 and 6, 4 and 7, and 5 and 8.

The maximum absorption wavelengths of bilayer and trilayer systems follow trends similar to those observed for single-layer structures, with absorption bands generally occurring within the 200-450 nm range. A particularly distinct behavior is observed in the stacked acene series, where a significant bathochromic shift occurs with an increasing number of aromatic rings. Specifically, λ_{max} progressively shifts toward longer wavelengths for structures such as anthracene-2, tetracene-3, pentacene-4, and hexacene-5 (**Figure IV.1-b/c**, red for 2L and blue for 3L). While the absorption maxima of the 2L and 3L naphthalene systems fall within the 200-300 nm range, those of the corresponding hexacene systems extend to approximately 800 nm.

GQD structures with "armchair" type edges

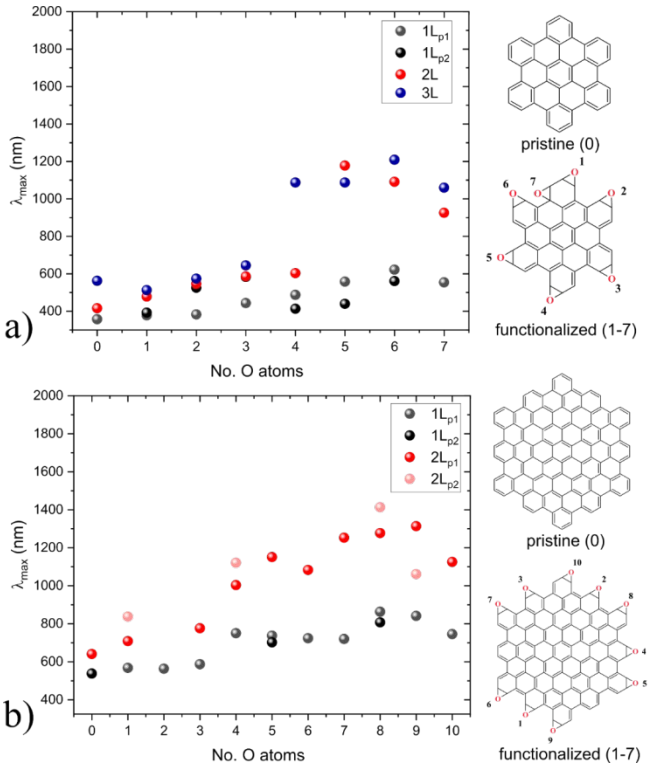


Figure IV.8. Graphical representation of maximum absorption wavelengths (λ_{max}) theoretically predicted for GQDh,ac: a) GQDh,ac,$C_{42}H_{18}$ with 1-7 epoxy groups and b) GQDh,ac,$C_{114}H_{30}$ with 1-10 epoxy groups, for monolayered (1L), bi-layered (2L) thriple-layered (3L) structures

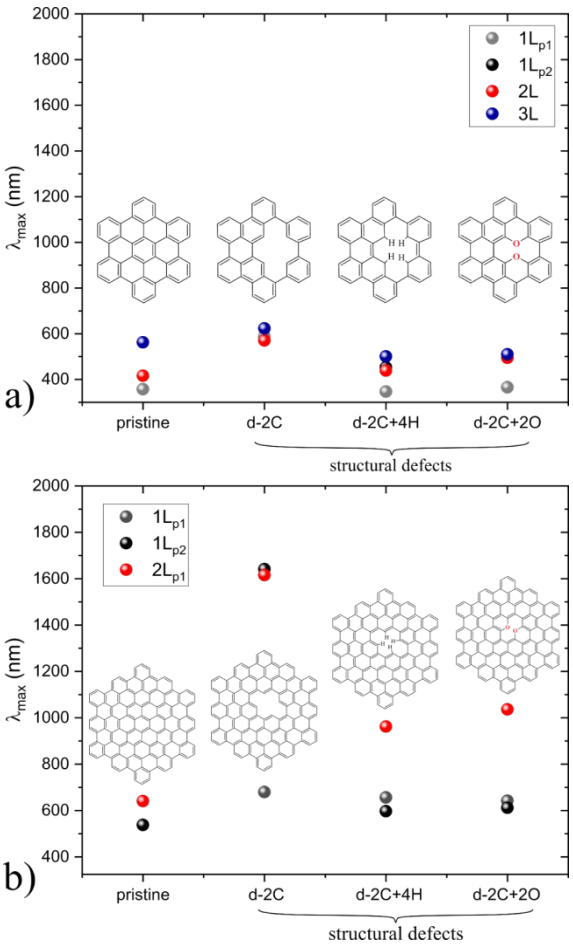


Figure IV.10. Graphical representation of maximum absorption wavelengths (λ_{max}) theoretically predicted for non-functionalized GQDh,ac and with structural defects for: a) GQDh,ac,$C_{42}H_{18}$ (1L, 2L and 3L) and b) GQDh,ac,$C_{114}H_{30}$ (1L and 2L). The defects have been introduced by the removal of 2 C vicinal atoms from the middle of the structure (d-2C), followed by the addition of 4 H atoms and 2 O atoms for the stabilization of the resulting structures (d-2C+4H and d-2C+2O).

The most pronounced bathochromic shifts in λ_{max} are observed for carbon-deficient structures (d-2C), in which the removal of two carbon atoms from the interior of the graphene plane substantially alters the extended π-electron conjugation, resulting in deviations from planarity and absorption maxima in the red and near-infrared (NIR) regions. This phenomenon is particularly pronounced in bilayer structures, where the previously discussed factors produce a cumulative effect on the electronic structure. The effect is most prominent in larger systems belonging to the GQDh,ac,$C_{114}H_{30}$ class.

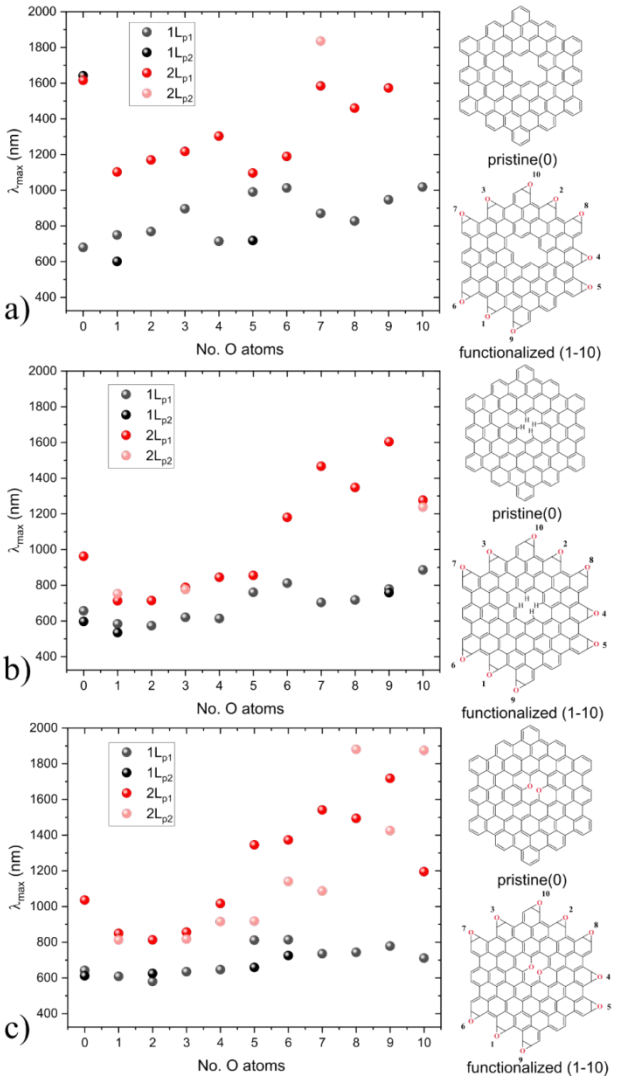


Figure IV.12. Graphical representation of the theoretically predicted maximum absorption wavelengths (λ_{max}) for single-layer (1L) and bilayer (2L) GQDh,ac,$C_{114}H_{30}$ structures containing structural defects and functionalized with 1-10 epoxy groups: (a) structures with defects generated by the removal of two carbon atoms, (b) structures with defects generated by the addition of four hydrogen atoms, and (c) structures with defects generated by the addition of two oxygen atoms.

For multilayer structures, a shift toward longer absorption wavelengths, reaching up to 1800 nm, was observed in bilayer (2L) and trilayer (3L) systems compared to single-layer (1L) structures. This behavior indicates a significant bathochromic shift into the near-infrared (NIR) region, associated with a decrease in the energy required for electronic transitions. The

overlap of π orbitals between adjacent layers promotes interlayer electronic coupling, leading to an effective extension of the conjugated system and a reduction in the energy gap between the frontier molecular orbitals.

This reduction enables the absorption of lower-energy radiation, consequently shifting the absorption maxima toward longer wavelengths. Furthermore, a second absorption maximum was observed in the TD-DFT spectra of both GQDh,ac,$C_{42}H_{18}$ ($1L_{p2}$) and GQDh,ac,$C_{114}H_{30}$ ($1L_{p2}$ and $2L_{p2}$) following the introduction of structural defects (Figure IV.10), most likely arising from charge-transfer (CT) interactions between graphene layers.

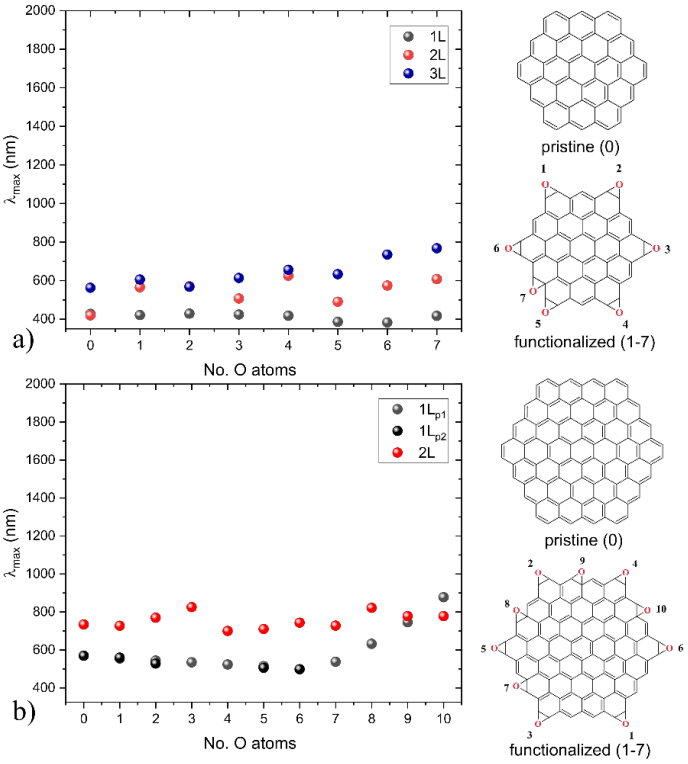


Figure IV.13. Graphical representation of the theoretically predicted maximum absorption wavelengths (λ_{max}) for the GQDh,zz class of structures: (a) $C_{54}H_{18}$ with 1-7 epoxy groups, considering single-layer (1L, gray dots), bilayer (2L, red dots), and trilayer (3L, blue dots) structures; (b) $C_{96}H_{24}$ with 1-10 epoxy groups, considering single-layer (1L, gray and black dots) and bilayer (2L, red dots) structures.

Compared to the previously discussed armchair-edge structures, the zigzag-edge structures (**Figure IV.13**) exhibit a narrower range of λmax variations, concentrated near the boundary between the ultraviolet and visible regions, with less pronounced fluctuations. This behavior is consistent with that reported by R. Zhang. (Chen et al., 2018) For the same type of GQDh,zz,$C_{54}H_{18}$ structures, the absorption wavelength remains virtually unchanged despite variations in the number of epoxy groups attached to the graphene plane. Furthermore, the variations in λ_{max} for single-layer (1L) zigzag structures are smaller (approximately 50 nm) than those observed for armchair-edge structures, and the wavelength profiles exhibit less pronounced fluctuations. To some extent, this behavior may help explain the differing trends reported in the literature, particularly those associated with variations in the degree of

oxidation. The limited variation in absorption wavelength between the pristine structure and systems functionalized with 1-7 epoxy groups may be advantageous for material design, particularly when modifications in solubility are required without significantly altering the optical absorption properties.

The stacking of graphene layers induces a bathochromic shift, similar to that observed for PAHs and GQDh,ac structures. Consequently, most absorption maxima of the bilayer GQDh,zz,$C_{54}H_{18}$ systems are located close to the visible-infrared limit, whereas the corresponding single-layer structures exhibit absorption primarily in the visible region. In contrast, the absorption maxima of the GQDh,zz,$C_{96}H_{24}$ systems extend into the near-infrared (NIR) region.

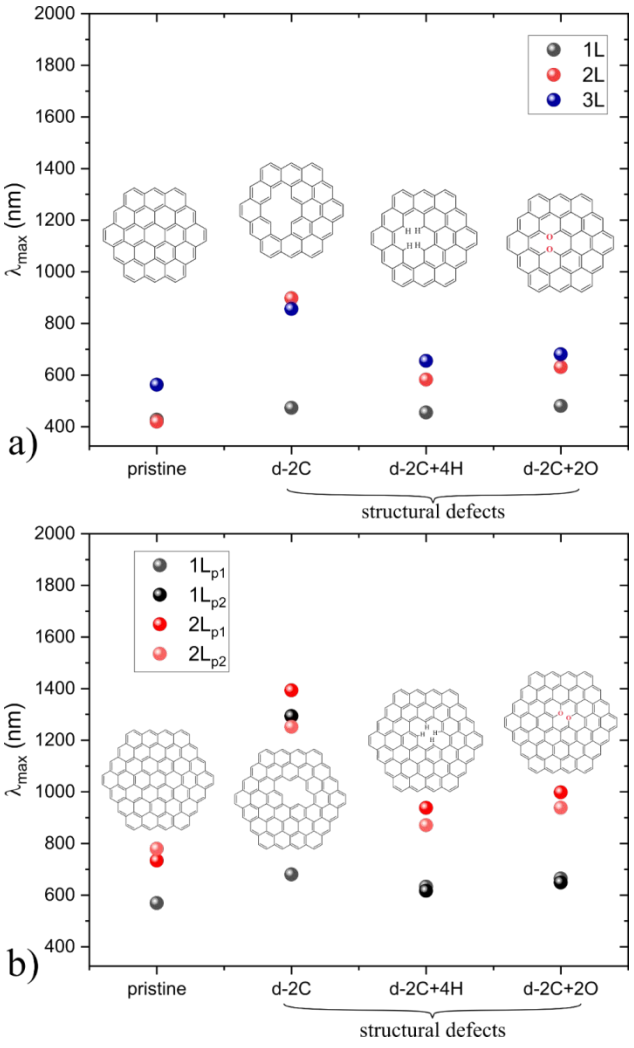


Figure IV.14. Graphical representation of the theoretically predicted maximum absorption wavelengths for the GQDh,zz class of structures: (a) GQDh,zz,C_54H_{18} (1L - monolayer, 2L - bilayer, 3L – triple layer) and (b) GQDh,zz,$C_{96}H_{24}$ (1L, $2L_{p1}$ $2L_{p2}$, in which p1, p2 are different relative positions between the graphitic layers), containing structural defects introduced by the removal of two carbon atoms (d-2C), followed by the addition of four hydrogen atoms (d-2C+4H) or two oxygen atoms (d-2C+2O) to stabilize the resulting structures.

Unlike the GQDh,zz,$C_{54}H_{18}$ structures, the GQDh,zz,$C_{96}H_{24}$ system exhibits a second absorption maximum in the single-layer configuration (indicated by gray circles, $1L_{p2}$). This secondary maximum was considered due to its emergence with increasing system size. As π-electron conjugation becomes more extensive, the number of molecular orbitals involved increases, while the energy gaps between them decrease. Consequently, nearly degenerate

electronic states may arise, potentially giving rise to additional electronic transitions or charge-transfer (CT) contributions. This behavior may be associated with $\pi \rightarrow \pi^*$ transitions involving CT character during electronic excitation.

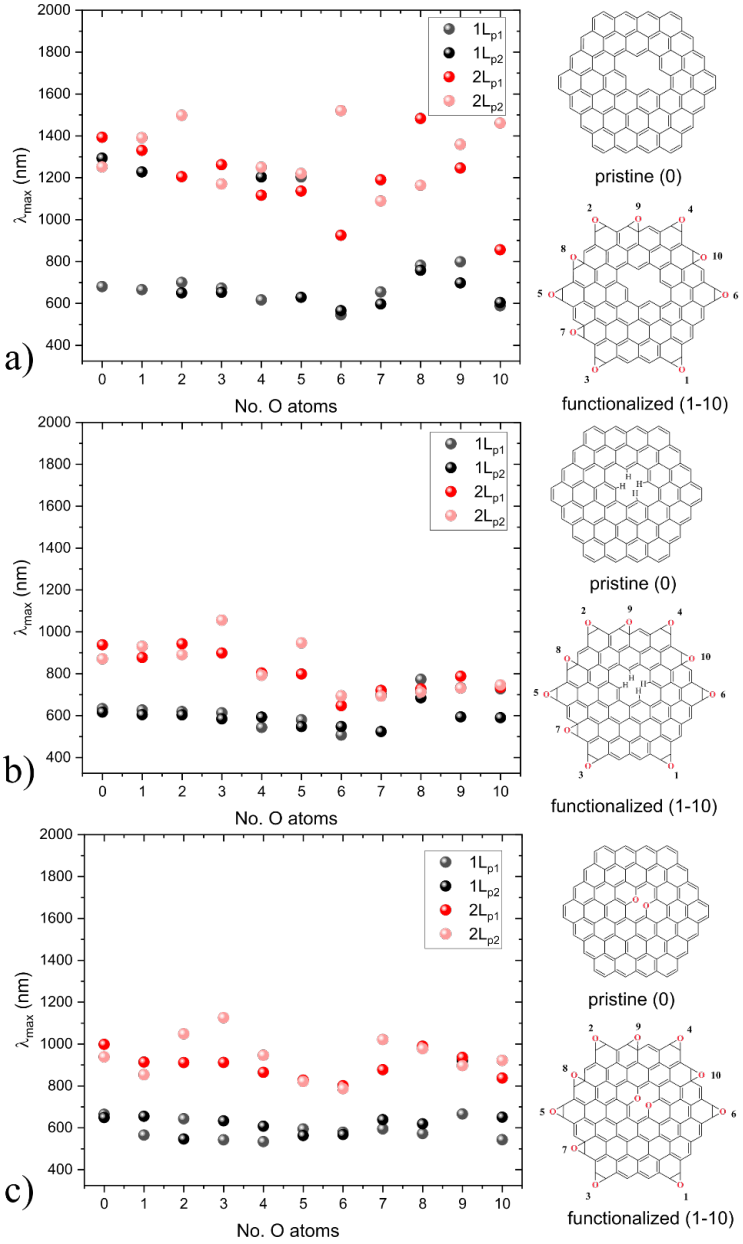


Figure IV.16. Graphical representation of the theoretically predicted maximum absorption wavelengths (λ_{max}) for single-layer (1L) and bilayer (2L) GQDh,zz,$C_{96}H_{24}$ structures containing structural defects and functionalized with 1-10 epoxy groups: (a) structures with defects generated by the removal of two carbon atoms, (b) structures with defects generated by the addition of four hydrogen atoms, and (c) structures with defects generated by the addition of two oxygen atoms.

The largest variations in λ_{max} (up to 1600 nm) are observed for the functionalized structures shown in **Figure IV.16-a**, in which two carbon atoms were removed. Splitting of the UV-Vis absorption bands is observed as a result of perturbations in electronic conjugation, similarly to the behavior of armchair-edge structures. This effect is particularly pronounced in bilayer (2L) systems, with a minimum absorption wavelength occurring when six epoxy groups are grafted onto the edges. This observation further highlights the role of achieving

complete molecular symmetry in inducing a hypsochromic shift in the absorption wavelength, associated with a more balanced electron density distribution across the graphene plane.

For GQDh,zz,$C_{96}H_{24}$, TD-DFT calculations revealed a similar tendency toward bathochromic shifts in bilayer structures (700-950 nm) compared to their single-layer counterparts (500-850 nm). In both single-layer and bilayer systems, the absorption wavelengths increase with the number of oxygen atoms located at the edges of the GQDh,zz,$C_{96}H_{24}$ unit (**Figure IV.12-b**) in comparison with the armchair structures (**Figure IV.16**). The pristine structure and systems containing up to seven oxygen atoms exhibit λ_{max} values in the 500-600 nm range, with a significant shift occurring as the number of oxygen atoms increases from 1 to 10.

The stabilizing effect of d-2C+4H and d-2C+2O defects is further highlighted in **Figures IV.12** and **IV.16**, where the variations of the absorption wavelength is limited, suggesting partial compensation for the electron density deficit. In contrast, functionalization with epoxy groups induces a hypsochromic shift in λ_{max} to values below 600 nm for single-layer structures and below 1000 nm for bilayer zigzag structures, representing a trend opposite to that observed for armchair-edge structures.

IV.4. Conclusions

Density functional theory (DFT) and time-dependent density functional theory (TD-DFT) were successfully employed to systematically investigate graphene quantum dot (GQD) structures of varying sizes, containing between 18 and 316 atoms, and to evaluate their maximum absorption wavelengths in the UV-Vis region. The study examined 23 polycyclic aromatic hydrocarbons (PAHs) and four hexagonal graphene quantum dot (GQDh) structures, including two with armchair edges (GQDh,ac,$C_{42}H_{18}$ and GQDh,ac,$C_{114}H_{30}$) and two with zigzag edges (GQDh,zz,$C_{54}H_{18}$ and GQDh,zz,$C_{96}H_{24}$).

The calculated maximum absorption wavelengths for the PAH series showed good agreement with experimental data. All PAH systems and smaller GQD structures (containing 48 and 54 carbon atoms) were investigated in single-layer, bilayer, and trilayer configurations, whereas the larger GQD structures (containing 96 and 114 carbon atoms) were examined in single-layer and bilayer configurations. The general trend in λ_{max} revealed a bathochromic (red) shift with increasing numbers of graphene layers.

The results demonstrate that the bathochromic shift in the maximum absorption wavelength is correlated with increasing molecular size and the presence of multiple graphene layers. Among all the investigated systems, single-layer PAH structures with fully conjugated

π-electron systems, such as tetracene, pentacene, and hexacene, exhibited the most intense electronic excitation bands. In contrast, helicene structures displayed lower excitation intensities (smaller oscillator strengths) due to their nonplanar geometries and disrupted π-conjugation.

Furthermore, the introduction of epoxy groups at the edges of four GQD structures, two with armchair edges (GQDac) and two with zigzag edges (GQDzz), revealed two distinct trends. Armchair-edge structures exhibited a continuous increase in absorption wavelength with increasing quantum dot size and the number of edge-attached epoxy groups, whereas zigzag-edge structures showed only minor deviations from the absorption wavelengths of their pristine counterparts upon the introduction of up to seven epoxy groups.

In multilayer configurations, a significant bathochromic shift toward the near-infrared (NIR) region was observed due to the presence of oxygen atoms. The introduction of structural defects into the graphene lattice resulted in either a bathochromic shift, when two carbon atoms were removed from the basal plane, or a hypsochromic shift, when the resulting carbon vacancies were stabilized by the addition of two oxygen atoms or four hydrogen atoms.

Additionally, the influence of functionalization with 1-10 edge-attached epoxy groups on the absorption wavelengths of GQD structures was investigated. The results indicate that edge functionalization induces different trends in armchair- and zigzag-edge structures. The introduction of up to seven epoxy groups along the edges of zigzag structures had only a minor effect on their optical properties, with limited variations in absorption wavelengths compared to the corresponding pristine GQDs. A hypsochromic effect was observed in both single-layer and bilayer systems. In contrast, increasing the number of attached functional groups to ten induced significant bathochromic shifts in the absorption wavelengths, associated with changes in molecular symmetry. For the two armchair-edge configurations, a pronounced bathochromic effect on λ_{max} was observed, correlated with both system size and the number of introduced oxygen atoms.

The introduction of structural defects generally induced a bathochromic shift in the absorption wavelengths of both single-layer and multilayer systems compared to defect-free, epoxy-functionalized structures. This effect was particularly pronounced for defects generated by removing two carbon atoms from the basal plane of GQD structures, both in pristine systems and in those containing edge-attached epoxy groups. The introduction of other types of defects exhibited a predominantly stabilizing effect, resulting in λmax values closer to those of the corresponding pristine structures. The influence of structural defects on optical

properties was more pronounced in larger GQD systems (GQDh,zz,$C_{96}H_{24}$ and GQDh,ac,$C_{114}H_{30}$).

These findings demonstrate that molecular size, edge configuration, degree of oxidation, number of graphene layers, and structural defects are effective parameters for tuning the optical properties of graphene quantum dots. They also highlight the potential of these materials for drug delivery applications through enhanced hydrophilicity and the introduction of structural cavities.

The **results** demonstrate that the optical properties of graphene quantum dots can be effectively tailored by modifying molecular size, number of layers, edge configuration, degree of functionalization, and structural defects within the graphene plane. The bathochromic shifts observed in certain systems, particularly functionalized multilayer structures and those containing basal-plane defects, indicate the possibility of extending their absorption range toward spectral regions relevant to biomedical applications. Furthermore, functionalization and defect engineering may contribute to increased hydrophilicity and the formation of structural cavities or active sites, highlighting the potential of these materials for bioimaging, drug delivery, and the controlled release of bioactive compounds.

GENERAL CONCLUSIONS

The present doctoral thesis aimed to investigate, using complementary in silico methods, molecular systems with potential applications in the encapsulation, delivery, and controlled release of active pharmaceutical ingredients or in bioimaging. The research focused on three structurally and functionally distinct classes of systems: β-cyclodextrin-based inclusion complexes, thermoresponsive poly(N-isopropylacrylamide) (PNIPAM) polymers, and graphene quantum dots (GQDs) with tunable optical properties. Despite the differences between these platforms, the results highlight the role of noncovalent interactions and molecular dynamics in complexation and the conformational response of polymers, as well as the influence of structural modifications on the optical properties of graphene-based systems.

Computational modeling enabled the investigation of these processes at the atomistic and electronic levels, complementing the available experimental data and providing mechanistic explanations and guidance for the rational design of materials with biomedical potential.

By integrating the findings obtained for the three classes of systems, the thesis highlights the importance of understanding, at the molecular level, the factors governing their properties. In cyclodextrin complexes, these factors control the orientation and reversibility of inclusion. In PNIPAM systems, they determine hydration, interchain association, and conformational transitions, whereas in GQD structures, functionalization and structural defects modify the electronic distribution and, consequently, the optical properties and potential adsorption sites. Although the methods employed differ, all studies demonstrate that local structural variations can induce significant changes in the overall behavior of the systems. This conclusion supports the need for molecular-level design of drug delivery systems and bioimaging materials, rather than optimization based exclusively on successive experimental trials.

In cyclodextrin complexes, these factors control the orientation and reversibility of inclusion. In PNIPAM systems, they determine hydration, interchain association, and conformational transitions, whereas in GQD structures, functionalization and structural defects modify the electronic distribution and, consequently, the optical properties and potential adsorption sites. Although the methods employed differ, all studies demonstrate that local structural variations can induce significant changes in the overall behavior of the systems. This conclusion supports the need for molecular-level design of drug delivery

systems and bioimaging materials, rather than optimization based exclusively on successive experimental trials.

A major contribution of the thesis lies in demonstrating the value of complementary theoretical methods and correlating their results with available experimental data. The simulations enabled the investigation of molecular mechanisms underlying the behavior of the studied systems, including competition between DMSO and propiconazole nitrate for occupancy of the β-cyclodextrin cavity, selective inclusion of the MPPC cation over the anion, the role of bridging hydrogen bonds in PNIPAM collapse, and the influence of edge type, functionalization, and structural defects on the optical absorption properties of GQD structures. Where available, experimental data provided a basis for evaluating theoretical predictions. Computational modeling complemented these findings by describing molecular orientations, conformational evolution, free energy profiles, and electronic transitions associated with optical absorption.

The interpretation of the results must consider the limitations of the methods employed. The findings depend on the force fields, solvent representation, system size, simulation duration, and extent of sampling, as well as on the functionals and basis sets used in quantum chemical calculations. Extrapolation to biological conditions requires additional validation.

Further research perspectives include the investigation of substituted cyclodextrins, functionalized or drug-loaded PNIPAM systems, and GQD models correlated with spectroscopic and biological data. Extending simulations to systems incorporating membranes, proteins, and environments resembling physiological conditions would enable the evaluation of molecular behavior under conditions more representative of biological systems.

Correlating these investigations with experimental studies would contribute to assessing the practical potential of the investigated systems.

Overall, the findings of this thesis demonstrate the value of *in silico* methods in identifying the factors influencing the stability, selectivity, stimuli responsiveness, and optical properties of the investigated systems. By providing mechanistic explanations and molecular-level insights, computational modeling can guide the selection of structures and experimental conditions, as well as the planning of subsequent experimental investigations. The thesis thus contributes to establishing a scientific foundation for the rational design of pharmaceutical formulations, stimuli-responsive systems, and materials with potential bioimaging applications through an improved understanding of the relationships between structure, environment, and properties.

SELECTED REFERENCES

Chen, S., Ullah, N., Wang, T., & Zhang, R. (2018). Tuning the optical properties of graphene quantum dots by selective oxidation: A theoretical perspective. *Journal of Materials Chemistry C*, *6*(25), 6875–6883. https://doi.org/10.1039/C8TC02083C

Fielding, L. (2000). Determination of Association Constants (*K*a) from Solution NMR Data. *Tetrahedron*, *56*(34), 6151–6170. https://doi.org/10.1016/S0040-4020(00)00492-0

Fifere, A., Marangoci, N., Maier, S., Coroaba, A., Maftei, D., & Pinteala, M. (2012). Theoretical study on β-cyclodextrin inclusion complexes with propiconazole and protonated propiconazole. *Beilstein Journal of Organic Chemistry*, *8*(1), 2191–2201. https://doi.org/10.3762/bjoc.8.247

Isac, D. L., Tîrnovan, P., Nicolescu, A., Fifere, A., Neamtu, A., & Pinteala, M. (2025). Cosolvent effects on the complexation of the antifungal propiconazole nitrate with β-cyclodextrin: A combined molecular dynamics and NMR study. *European Journal of Pharmaceutical Sciences*, *213*, 107248. https://doi.org/10.1016/j.ejps.2025.107248

Langer, M., Hrivnák, T., Medved', M., & Otyepka, M. (2021). Contribution of the Molecular Fluorophore IPCA to Excitation-Independent Photoluminescence of Carbon Dots. *The Journal of Physical Chemistry C*, *125*(22), 12140–12148. https://doi.org/10.1021/acs.jpcc.1c02243

Li, Z., Fan, J., Tong, C., Zhou, H., Wang, W., Li, B., Liu, B., & Wang, W. (2019). A Smart Drug-Delivery Nanosystem Based on Carboxylated Graphene Quantum Dots for Tumor-Targeted Chemotherapy. *Nanomedicine*, *14*(15), 2011–2025. https://doi.org/10.2217/nnm-2018-0378

Marangoci, N., Mares, M., Silion, M., Fifere, A., Varganici, C., Nicolescu, A., Deleanu, C., Coroaba, A., Pinteala, M., & Simionescu, B. C. (2011). Inclusion complex of a new propiconazole derivative with β-cyclodextrin: NMR, ESI–MS and preliminary pharmacological studies. *Results in Pharma Sciences*, *1*(1), 27–37. https://doi.org/10.1016/j.rinphs.2011.07.001

Pricope, G., Ursu, E. L., Sardaru, M., Cojocaru, C., Clima, L., Marangoci, N., Danac, R., Mangalagiu, I. I., Simionescu, B. C., Pinteala, M., & Rotaru, A. (2018). Novel cyclodextrin-based pH-sensitive supramolecular host–guest assembly for staining acidic cellular organelles. *Polymer Chemistry*, *9*(8), 968–975. https://doi.org/10.1039/C7PY01668A

Tirnovan, P., Isac, D. L., Man, I. C., Puf, R. C., Dascalu, I. A., Coroaba, A., Marangoci, N. L., Cibotariu, N. I., Ciuhodaru, T., Ania, C. O., & Pinteala, T. (2026). Extensive TD-DFT investigation of the absorption wavelength in single and multilayer polycyclic aromatic hydrocarbons/graphene quantum carbon dots. *Surfaces and Interfaces*, *98*, 110526. https://doi.org/10.1016/j.surfin.2026.110526

Tirnovan, P., Isac, D. L., Marangoci, N. L., Nicolescu, A., Coroaba, A., Cretu, B., Laaksonen, A., Neamtu, A., & Pinteala, T. (2026). Supramolecular insights into the complexation of β-Cyclodextrin for alopecia treatment using the mixed cation/anion active principle. *Carbohydrate Polymer Technologies and Applications*, *14*, 101155. https://doi.org/10.1016/j.carpta.2026.101155

APPENDIX 1 DISSEMINATION OF RESEARCH RESULTS

Articles Published in ISI-Indexed Scientific Journals Whose Results Form the Basis of This Doctoral Thesis:

1. Isac, D. L., **Tirnovan, P.**, Nicolescu, A., Fifere, A., Neamtu, A., & Pinteala, M. (2025). Cosolvent effects on the complexation of the antifungal propiconazole nitrate with β-cyclodextrin: A combined molecular dynamics and NMR study. *European Journal of Pharmaceutical Sciences*, 213, 107248. https://doi.org/10.1016/j.ejps.2025.107248. (**FI = 5,1, Q = Q1**) (AIS = 0,712, Q = Q1)

2. **Tirnovan, P.**, Isac, D. L., Marangoci, N. L., Nicolescu, A., Coroaba, A., Cretu, B., Laaksonen, A., Neamtu, A., & Pinteala, T. (2026). Supramolecular insights into the complexation of β-Cyclodextrin for alopecia treatment using the mixed cation/anion active principle. *Carbohydrate Polymer Technologies and Applications*, 14, 101155. https://doi.org/10.1016/j.carpta.2026.101155. (**FI = 7.6, Q = Q1**) (AIS = 0.861 , Q = Q1).

3. **Tirnovan, P.**, Isac, D. L., Man, I. C., Puf, R., Dascalu, A., Coroaba, A., Marangoci, N. L., Cibotariu, N., Ciuhodaru, T., Ania, C. O., Pinteala, T. (2026). Extensive TD-DFT Investigation of the Absorption Wavelength in Single and Multilayer Polycyclic Aromatic Hydrocarbons/Graphene Quantum Carbon Dots. *Surfaces and Interfaces,* 98, 110526. https://doi.org/10.1016/j.surfin.2026.110526. (**FI = 6,0, Q = Q1**) (AIS = 0,720, Q = Q1).

4. Bacaita, E. S., **Tirnovan, P.**, Laaksonen, A., Mocci, F. (2026). Toward Reliable LCST Prediction of PNIPAM: The Influence of Water Model and Multi-Chain Interactions. *Journal of Physical Chemistry B.* (**FI = 3,2, Q = Q2**) (AIS = 0,660, Q = Q2).

Databases:

1. Isac, D. L., Man, I. C., **Tirnovan, P.**, (2026). Extensive TD-DFT Investigation of the Absorption Wavelength in Single and Multilayer Polycyclic Aromatic Hydrocarbons/Graphene Quantum Carbon Dots. *Zenodo*, https://doi.org/10.5281/zenodo.22525788.

During the doctoral studies, the PhD student Tîrnovan Petru was a member of the implementation teams of the following research projects:

1. „Intelligent systems for cancer diagnosis and treatment - **IntelDots**" PNRR-III-C9-2022-I8-291;

2. „**BioMat4CAST** - "Petru Poni" Institute of Macromolecular Chemistry Multi-Scale In Silico Laboratory for Complex and Smart Biomaterials" Grant Agreement No 101086667

Research Internships and Mobility Programs Undertaken During Doctoral Studies:

1. Recent Advances in Computational Biophysics (RACB): Methods and Applications, Forschungszentrum Jülich, Germany, 3rd -7th of February **2025**.

2. NGMM 2026 Next-Generation Modelling Summer School, Sardinia, Italy, 27th-31st of July **2026**.

Participation in International and National Scientific Conferences:

Oral Communications

1. *In silico* studies of a novel amphiphilic graft conjugated polymer for biomedical applications; **P. Tirnovan**, F. Mocci, T. Vasiliu, L. Cianga, I. Cianga, M. Pinteala, A. Laaksonen. *MacroYouth 2021*, ICMPP - *Open door to the future scientific communications of young researchers, second edition,* Iași, România; 19th of November **2021**.

2. Study of Radical Species Formation from Urocanic Acid under UV Irradiation: an Experimental and Theoretical Analysis of its Role in Skin Cancer; **P. Tirnovan**, D. L. Isac, M. Silion, A. Coroaba, T. Rusu, M. Pinteala, A. Laaksonen. *PolyChar'30: PolyChar World Forum on Advanced Materials 30 Edition*, Iași, România, 11th -13th of November **2024**.

3. Unveiling the role or urocanic acid in the formation of skin cancer; **P. Tirnovan**, D. L. Isac, M. Silion, A. Coroaba, A. Laaksonen, M. Pinteala, *MacroYouth 2025, Open door to the future scientific communications of young researchers, 6th edition,* Iasi, Romania, 19th of November **2025**. (**Third Prize**)

4. BioMat4CAST Multi-Scale In Silico Laboratory for Complex and Smart Biomaterials, **P. Tirnovan**, R. Puf, D. L. Isac, *ICUB-IBAR Joint Workshop; Current Topics in Molecular Biosciences*; Bucharest, Romania, 27th of November **2025**.

Posters

1. *In silico* Investigation of an Amphiphilic Graft Conjugated Polymer. A Comparative Study of Different Solvation Models; **P. Tirnovan**, F. Mocci, T. Vasiliu, R. Puf, T. Rusu, M. Pinteală, A. Laaksonen, *PolyChar'30: PolyChar World Forum on Advanced Materials 30 Edition,* Iasi, Romania, 11th -13th of November **2024**.

2. Urocanic Acid and its Role in skin Cancer Under UV-irradiation. A Combined Experimental and Theoretical Study; **P. Tirnovan**, D. L. Isac, M. Silion, A. Coroaba, T. Rusu, M. Pinteala, F. Mocci, A. Laaksonen, *Recent Advances in Computational Biophysics: Methods and Applications*, Forschungszentrum Jülich, Germany, 3rd -7th of February **2025**.

3. Simulating molecular systems with peculiar fluorescence. A case study of lysine; P. Tirnovan, C. M. Carbonaro, L. V. Engelbrecht, A. Laaksonen, T. Rusu, M. Pinteala, F. Mocci*, COST COSY Training School, Exploring Confined Environments with Polymers, Ionic Liquids, and Deep Eutectic Solvents: Predicting Emerging Applications through Modeling and Advanced Experiments*, Iasi, Romania, 8th -9th of May **2025**. (**Third Prize**)

4. Mechanistic insights înto the complexation mechanism of an organic salt drug with cyclodextrin; **P. Tirnovan**, D.-L. Isac, N.-L. Marangoci, A. Neamtu, A. Laaksonen, M. Pinteala, *NGMM 2026 Next-Generation Modelling Summer School*, Sardinia, Italy, 27th-31st of July **2026**.

5. Inclusion of an Organic Salt Drug Formulation with β-Cyclodextrin for the Treatment of Alopecia. A Theoretical and Experimental Investigation; **P. Tirnovan**, D.-L. Isac, N.-L. Marangoci, A. Nicolescu, A. Coroaba, A. Neamtu, B. Cretu, A. Laaksonen, T. Pinteala, *The 5th European Symposium on Chemical Bonding (CBOND2026)*, Bruxelles, Belgium, 8th-11th of September **2026**.